AF NETF GRAPHITE STANDARD PILE

TECHNICAL DOCUMENTARY REPORT No. WADD-TR-61-174

MARCH 1962

NUCLEAR ENGINEERING TEST FACILITY
DIRECTORATE OF ENGINEERING TEST
AERONAUTICAL SYSTEMS DIVISION
AIR FORCE SYSTEMS COMMAND
WRIGHT-PATTERSON AIR FORCE BASE, OHIO

Project No. 7001, Task No. 70012

NOTICES

When Government drawings, specifications, or other data are used for any purpose other than in connection with a definitely related Government procurement operation, the United States Government thereby incurs no responsibility nor any obligation whatsoever; and the fact that the Government may have formulated, furnished, or in any way supplied the said drawings, specifications, or other data, is not to be regarded by implication or otherwise as in any manner licensing the holder or any other person or corporation, or conveying any rights or permission to manufacture, use, or sell any patented invention that may in any way be related thereto.

ASTIA release to OTS not authorized.

Qualified requesters may obtain copies of this report from the Armed Services Technical Information Agency, (ASTIA), Arlington Hall Station, Arlington 12, Virginia.

Copies of ASD Technical Reports and Technical Notes should not be returned to the Aeronautical Systems Division unless return is required by security considerations, contractual obligations, or notice on a specific document.

Aeronautical Systems Division, Wright-
Patterson Air Force Base, Ohio. Rpt. No.
WADD-TR-61-174. AF NETF GRAPHITE STANDARD
PILE. Final report, Mar 62, 51p incl. illus.,
tables.

Unclassified report

The design, fabrication, and calibration of
a graphite standard pile installed at AF
NETF is described. The pile is constructed
from AGOT graphite stringers 4" x 4" x 50".
Eighteen layers of stringers are used to
build a pile 4' x 4' x 6'. The neutrons
originate from a five curie Pu-Be source
having an 8.86 x 10⁶ neutrons/sec source

(over)

1. Standard pile
2. Neutrons
3. Neutron flux
   measurement
4. Foil measurement
I. AFSC Project 7001
   Task 7OO12
II. Contract AF 33
    (616)-5997
III. American Machine
     and Foundry Co.,
     Alexandria, Va.
IV. A. W. Carriker
    A. J. Calio, J. S.
    Strano
V. Not aval fr OTS

VI. In ASTIA collec-
    tion

strength. The thermal neutron flux, absolute-
ly calibrated against the National Bureau of
Standards source NBS-A, is given. The foil
data, calibration procedures and neutron
flux spatial distribution are presented in
detail. The spatial flux dependency is
treated theoretically by solution of the age-
diffusion equation.

Aeronautical Systems Division, Wright-Patterson Air Force Base, Ohio. Rpt. No. WADD-TR-61-174. AF NETF GRAPHITE STANDARD PILE. Final report, Mar 62, 51p incl. illus., tables.

Unclassified report

The design, fabrication, and calibration of a graphite standard pile installed at AF NETF is described. The pile is constructed from AGOT graphite stringers 4" x 4" x 50'. Eighteen layers of stringers are used to build a pile 4' x 4' x 6'. The neutrons originate from a fiye curie Pu-Be source having an 8.86×10^6 neutrons/sec source

(over)

strength. The thermal neutron flux, absolutely calibrated against the National Bureau of Standards source NBS-A, is given. The foil data, calibration procedures and neutron flux spatial distribution are presented in detail. The spatial flux dependency is treated theoretically by solution of the age-diffusion equation.

1. Standard pile
2. Neutrons
3. Neutron flux measurement
4. Foil measurement
I. AFSC Project 7001 Task 70012
II. Contract AF 33 (616)-5997
III. American Machine and Foundry Co., Alexandria, Va.
IV. A. W. Carriker
A. J. Calio, J. S. Strano
V. Not aval fr OTS

VI. In ASTIA collection

Aeronautical Systems Division, Wright-
Patterson Air Force Base, Ohio. Rpt. No.
WADD-TR-61-174. AF NETF GRAPHITE STANDARD
PILE. Final report, Mar 62, 51p incl. illus.,
tables.

Unclassified report

The design, fabrication, and calibration of
a graphite standard pile installed at AF
NETF is described. The pile is constructed
from AGOT graphite stringers 4" x 4" x 50".
Eighteen layers of stringers are used to
build a pile 4' x 4' x 6'. The neutrons
originate from a five curie Pu-Be source
having an 8.86 x 10⁶ neutrons/sec source

(over)

1. Standard pile
2. Neutrons
3. Neutron flux
   measurement
4. Foil measurement
I. AFSC Project 7001
   Task 70012
II. Contract AF 33
   (616)-5997
III. American Machine
   and Foundry Co.,
   Alexandria, Va.
IV. A. W. Carriker
   A. J. Calio, J. S.
   Strano
V. Not aval fr OTS

VI. In ASTIA collec-
tion

strength. The thermal neutron flux, absolute-
ly calibrated against the National Bureau of
Standards source NBS-A, is given. The foil
data, calibration procedures and neutron
flux spatial distribution are presented in
detail. The spatial flux dependency is
treated theoretically by solution of the age-
diffusion equation.

Aeronautical Systems Division, Wright-Patterson Air Force Base, Ohio. Rpt. No. WADD-TR-61-174. AF NETF GRAPHITE STANDARD PILE. Final report, Mar 62, 51p incl. illus., tables.

Unclassified report

The design, fabrication, and calibration of a graphite standard pile installed at AF NETF is described. The pile is constructed from AGOT graphite stringers 4" x 4" x 50". Eighteen layers of stringers are used to build a pile 4' x 4' x 6'. The neutrons originate from a five curie Pu-Be source having an 8.86×10^6 neutrons/sec source

(over)

1. Standard pile
2. Neutrons
3. Neutron flux measurement
4. Foil measurement
I. AFSC Project 7001 Task 70012
II. Contract AF 33 (616)-5997
III. American Machine and Foundry Co., Alexandria, Va.
IV. A. W. Carriker
    A. J. Calio, J. S. Strano
V. Not aval fr OTS

VI. In ASTIA collection

strength. The thermal neutron flux, absolutely calibrated against the National Bureau of Standards source NBS-A, is given. The foil data, calibration procedures and neutron flux spatial distribution are presented in detail. The spatial flux dependency is treated theoretically by solution of the age-diffusion equation.

FOREWORD

This report was prepared by American Machine and Foundry Company, Alexandria Division, on USAF Contract AF33 (616)-5997 under Task No. 70012 of Project No. 7001, "AF NETF Graphite Standard Pile." The work was administered under the direction of Air Force Nuclear Engineering Test Facility, Aeronautical Systems Division. Mr. Henry P. Kalapaca was project engineer for the laboratory.

This report covers work conducted from July 1958 to November 1960.

Basic design and computational work on this contract commenced 15 July 1958 with Mr. H. M. Childers as project engineer. Design was completed and approved by 10 December 1958. All material was fabricated and ready for shipment by 1 July 1959 and was stored until shipping orders were received. On 1 August 1959 Mr. A. J. Calio became project engineer. The pile materials were shipped and the completed pile was installed by July 1960 and calibrated in September 1960. On 1 August 1960 Mr. A. W. Carriker assumed project supervision.

Among those who assisted in this program were Mr. A. S. DeAngelo, Mr. T. K. Hannan, and Mr. J. S. Strano, all of American Machine and Foundry Company and Mr. A. N. Fasano, Lt. R. P. Kennel and Mr. C. W. Garrett of the AF NETF. Final corrections of copy and publication arrangements were handled by Mr. J. A. Dooley of AF NETF.
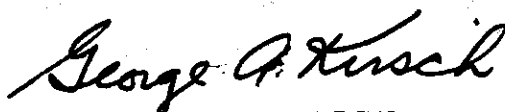
This report concludes the work on contract AF 33(616)-5997.

ABSTRACT

The design, fabrication, and calibration of a graphite standard pile installed at AF NETF is described. The pile is constructed from AGOT graphite stringers 4" x 4" x 50". Eighteen layers of stringers are used to build a pile 4' x 4' x 6'. The neutrons originate from a five curie Pu-Be source having an 8.86×10^6 neutrons/sec source strength. The thermal neutron flux, absolutely calibrated against the National Bureau of Standards source NBS-A, is given. The foil data, calibration procedures and neutron flux spatial distribution are presented in detail. The spatial flux dependency is treated theoretically by solution of the age-diffusion equation.

PUBLICATION REVIEW

This report has been reviewed and is approved.

George A. Kirsch

GEORGE A. KIRSCH
Colonel, USAF
Asst Deputy Commander/Test and Support

CONTENTS

LIST OF ILLUSTRATIONS

LIST OF TABLES

I. INTRODUCTION

Owing to the need for an accurately calibrated source of thermal neutrons a Graphite Standard Pile was designed, fabricated, installed, and calibrated at the Air Force Nuclear Engineering Test Facility. The principal use for such a pile is to serve as an absolute standard for comparative determinations of the magnitude of other thermal neutron fluxes. In addition to providing a known source of thermal neutrons in which monitoring foils may be calibrated, the pile may be used to accurately determine the absolute efficiency of nuclear counting equipment; for low level thermal neutron radiation studies; for calibrating thermal neutron detection devices such as boron trifluoride detectors, scintillation detectors, and personnel monitoring dosimeters; for the measurement of thermal neutron cross sections; and for investigating neutron slowing down and diffusion in graphite. The special design of this graphite pile provides grooves to the exterior of the pile for insertion of devices with connecting cables or tubing so that experiments may be conducted conveniently. A fast neutron flux is available through a void that is formed by removal of a portion of graphite. The neutron source for this graphite pile is an 79.79 gram plutonium-beryllium source having a source strength of about 8.86×10^6 neutrons/sec. A spectral distribution of the source is shown in a later section.

The graphite pile was calibrated using the foil activation method. The thermal neutron flux at one position in the graphite pile was compared with the standard flux maintained by the National Bureau of Standards. This involved irradiating gold foils in both the graphite pile and the NBS facility and counting these foils in the same counting apparatus. The flux at positions in the pile other than the standard position was determined by comparison with the standard position using the foil activation method.

Cadmium covered and bare indium foils were irradiated, and consequently the indium resonance activity was measured. The age of the source neutrons in graphite ($\tau = 326$ cm^2) was obtained from the slope of the curve of the indium resonance activity as a function of the square of distance from the source. Computing the slope of the curve of the observed thermal neutron induced activity as a function of the distance from the source a relaxation length of 24.2cm was obtained. Both of these values are in excellent agreement with the published data.

Manuscript released by the authors December 1960 for publication as a WADD Technical Report.

An exact solution to the age diffusion equation has been found for the geometry of the AFNETF graphite standard pile. The solution considers a point source in a rectangular solid of infinite length. The complete derivation of these solutions is given in Appendix I.

II. COMPARISON OF NEUTRON FLUXES USING
THE FOIL ACTIVATION METHOD

If a thin foil of a material having a thermal neutron capture cross section that varies inversely as the neutron velocity, v, is irradiated in a field of thermal neutrons, then the rate at which neutrons are captured by this foil is given by

$$c = \sum_i n_i \, v_i \sigma_i \, N \tag{1}$$

where n_i is the density of the neutrons of velocity, v_i; σ_i is the microscopic capture cross section for neutrons of velocity, v_i; and N is the number of atoms in the foil. Since σ varies as $1/v$, the product $v_i \sigma_i$ is a constant. If the cross section, σ_o, for the most probable speed, v_o, in a Maxwellian distribution is measured, the above expression can be written

$$c = \sigma_o v_o N \sum_i n_i = (n v_o) \sigma_o N \tag{2}$$

where n is the neutron density at the foil. The flux $(n v_o)$ is commonly referred to as the 2200 meter flux, since 2200 m/sec is the most probable speed of a neutron in a Maxwellian distribution at 20°C. It is important to note that the neutron density can be determined independently of velocity distribution provided the velocity of the neutrons is restricted to the region of $1/v$ variation of the capture cross section.

Since the number of atoms, N, in the foil is usually many orders of magnitude greater than the number of atoms in the foil that is activated by neutron capture, the product, $N\sigma$, can be considered as being a fixed quantity for a given foil and neutron energy spectrum. The absolute value of $N\sigma$ need not be known when the comparison technique is employed to measure the magnitude of neutron fluxes with very similar energy spectra.

A foil being irradiated in a constant neutron flux is said to be saturated when the rate of decay of activated nuclei is equal to the rate of production. For all practical purposes a foil may be considered to be saturated after an irradiation period of ten times the half-life of the radioisotope formed by neutron capture. At saturation, the rate of production, c, equals the rate of decay which will be designated as A_s. Equation (2) can be rewritten as

$$A_s = (nv_o)\sigma_o N \tag{3}$$

where A_s is in units of activated nuclei decaying per unit time.

When the activity of the foil is measured with an appropriate counting system, the saturated-activity counting rate, R_s, is related to the saturated activity, A_s, by the relationship

$$R_s = \epsilon A_s \tag{4}$$

where ϵ is the over-all efficiency of the counting system for the particular foil and geometrical configuration.

If the performance of the counting system is stable and the foil-detector geometrical configuration is reproducible, an expression can be written

$$R_s = nv_o \epsilon N\sigma_o \tag{5}$$

where all terms except n are constant, provided the neutrons that irradiated the foil are of velocities such that the cross section varies as the reciprocal of the velocity. This expression readily lends itself to comparing the magnitude of neutron fluxes with similar spectra, and it can be rewritten

$$\frac{R_s}{nv_o} = \epsilon N\sigma_o = \text{constant} \tag{6}$$

With a value of $(R_s)_1$ measured for a known flux, $(nv_o)_1$, the value of an unknown flux, $(nv_o)_2$, is determined by measuring $(R_s)_2$ and applying it in the expression

$$\frac{(R_s)_1}{(nv_o)_1} = \frac{(R_s)_2}{(nv_o)_2} = \text{constant} \tag{7}$$

The most common technique employed for determining the saturated activity counting rate of a foil is to observe an accumulated number of counts during some finite counting interval. Also, it is often not practical to irradiate a foil for a period sufficiently long to reach saturation. The derivation of the expression for determining the saturated-activity counting rate from an observed accumulated number of counts is shown in detail in the work by Childers and Graves.[1] The expression that relates the saturated activity counting

---

[1]H. M. Childers and J. D. Graves, "The Neutron Converter: Thermal Neutron Flux Calibration," N.R.L. Formal Report No. 4575, 1, August 1955.

rate, R_s, to an accumulated number of counts recorded with a counting apparatus may be expressed as

$$R_s = \frac{\lambda C(t_c) e^{\lambda t_w}}{(1-e^{-\lambda t_e})(1-e^{-\lambda t_c})} - \frac{R_o e^{-\lambda t_e}}{(1-e^{-\lambda t_e})} \qquad (8)$$

where λ is the decay constant of the radionuclide formed by neutron capture in the foil material, $C(t_c)$ is the recorded number of counts during the counting interval, t_e is the time interval that the foil was irradiated, t_c is the counting interval, t_w is the elapsed time between the end of the irradiation interval and the start of the counting interval, and R_o is the counting rate of the foil at the start of the irradiation interval, assuming the foil is partially activated at the start of the irradiation interval. Combining equations (6) and (8) yields the expression

$$\epsilon N \sigma_o = \frac{1}{n v_o} \left[\frac{\lambda C(t_c) e^{\lambda t_w}}{(1-e^{-\lambda t_e})(1-e^{-\lambda t_c})} - \frac{R_o e^{-\lambda t_e}}{(1-e^{-\lambda t_e})} \right] \qquad (9)$$

when can be used when a particular foil is used to compare neutron fluxes with similar spectra.

In comparing thermal neutron fluxes that have spectra such that the capture cross section of the foil material for part of the neutrons does not vary as the reciprocal of the neutron velocity, it is necessary to apply correction factors which will permit specifying the effective value of the flux in terms of some conventional energy distribution. The 2200 meter flux is the most commonly specified thermal neutron flux.

A detecting foil will act as a "sink" for neutrons and will distort the flux in a region near the foil. The extent of this region depends on the size and cross section of the foil and on the mean free path of neutrons in the surrounding material. Furthermore, unless the foil is extremely thin the outer layers of atoms in the foil will partially shield the atoms of the inner layers. When a foil is used to compare neutron fluxes with similar spectra in moderating media of the same material, the flux distortion in the medium and self-shielding in the foil will essentially be the same for all measurements. A comprehensive theoretical evaluation of the problem of thermal neutron flux depression has been reported by Ritchie and Eldridge.[2] An excellent discussion of the experiment procedure for determining this correction factor is shown in the work by Bebbs

---
[2] R. H. Ritchie and H. B. Eldridge, "Thermal Neutron Flux Depression by Absorbing Foils," Nuc. Sci. and Eng., 8, (4), 300, October 1960.

and Price.[3]

In order to measure the thermal neutron flux in the presence of neutrons with energies or velocities greater than the region of $1/v$ variation in the cross section of the detecting foil, a common practice is to irradiate a foil bare and with a cadmium cover at the point of interest. Since cadmium has an extremely large cross section for neutrons with energies less than about 0.4 ev., irradiating the foil inside a cadmium cover results in an activity in the foil that is induced only by neutrons with energies greater than about 0.4 ev. The activity of the foil after it has been irradiated bare results from neutrons of all energies. The difference between the bare and cadmium covered foil activities is approximately the activity due to thermal neutrons only. Correction factors must be applied to measurements made with bare and cadmium covered foils since the cadmium cross section is not truly a step function and any cadmium cover is neither truly transparent to neutrons greater than 0.4 ev, nor opaque to thermal neutrons.[3,4,5,6] The correction factors depend on the thickness of the cadmium cover, the dimensions of the foil, the cross section of the foil material, the medium in which the measurements are being made, and the spectrum of the neutrons being measured.

The total observed saturated activity count rate of a cadmium covered foil, $R_{cd}^T(\text{obs})$, is composed of two components--the observed activity due to epicadmium neutrons, $R_{cd}^e(\text{obs})$, and the observed activity due to thermal neutrons, $R_{cd}^{th}(\text{obs})$, where $R_{cd}^e(\text{obs})$, and $R_{cd}^{th}(\text{obs})$ are observed from Figure 5 explained in the next paragraph.

$$R_{cd}^T(\text{obs}) = R_{cd}^e(\text{obs}) + R_{cd}^{th}(\text{obs}) \qquad (10)$$

[3]E. H. Bebbs and H. Clay Price, Jr., "Naval Research Laboratory Research Reactor, Part VIII - Neutron Flux Measurements and Power Determination," N.R.L. Formal Report No. 5196, November 28, 1958.

[4]J. W. Kunstadter, "A Correction Factor to be Applied to the Activity of Neutron-Activated Cadmium Covered Indium Foils," Phys. Rev., 78, 484, 1950.

[5]C. W. Tittle, "Slow Neutron Detection by Foils," Nucleonics, 8, (6), 5 June 1959, and Nucleonics, 9, (1), 60, July 1951.

[6]D. H. Martin, "Correction Factors for Cd-Covered-Foil Measurements," Nucleonics, 13, (3), 52, March 1955.

The experimental technique for determination of the correction factors for the cadmium covered foil measurements involves irradiating matched foils that are covered with different thicknesses of cadmium in the same neutron flux. A semilog plot is made of the total observed saturated activity counting rate of these foils vs. cadmium cover thickness from which correction factors for $R_{cd}^e(obs)$ and $R_{cd}^{th}(obs)$ may be obtained. A typical curve determined from such a plot of experimental data is shown in Section IV as Figure 6.

To obtain the correction factor that is used to determine R_{cd}^e (true) from $R_{cd}^e(obs)$, the count rate obtained by extrapolation of the straight-line portion of the curve of Figure 6 to zero cadmium cover thickness is divided by the count rate taken from the extrapolated straight-line for the cadmium cover thickness of interest. This correction factor, F_{cd}, compensates for the fact that the cross section of cadmium is not truly a step function and that the cadmium cover absorbs part of the neutrons with energies greater than the cadmium "cut-off" (approx. 0.4 ev). Thus the observed epicadmium activity is always lower than the true epicadmium activity would be if the cadmium cover were perfectly transparent to epicadmium neutrons. The product of the correction factor, F_{cd}, and the observed epicadmium count rate, $R_{cd}^e(obs)$, yields the true count rate, $R_{cd}^e(true)$, that would exist if none of the epicadmium neutrons had been absorbed in the cadmium cover.

$$R_{cd}^e(true) = F_{cd} \quad R_{cd}^e(obs) \tag{11}$$

To obtain the correction factor that compensates for the fact that the cadmium cover is not completely opaque to neutrons of energies less than the cadmium "cut-off", a semilog plot is made of the relative observed thermal neutron or subcadmium produced activity of a set of matched foils with cadmium covers versus cadmium cover thickness. This correction factor is the thermal leakage factor X and is defined as the ratio of the observed thermal neutron induced activity of the cadmium covered foil, $R_{cd}^{th}(obs)$, to the observed thermal neutron induced activity in the bare foil, R_b^{th}.

$$X = \frac{R_{cd}^{th}(obs)}{R_b^{th}} \tag{12}$$

Such a plot of X is shown in Figure 7, and the curve is obtained from a plot of data such as is shown in Figure 6. The difference between the experimental points, $R_{cd}^T(obs)$, and the points on the extrapolated straight-line, $R_{cd}^e(obs)$, is divided by the thermal part of zero cadmium thickness foil, R_b^{th}, and plotted against cadmium cover thickness.

The total saturated activity count rate of a bare foil, R_b^T, is composed of two components--the activity resulting from thermal neutrons, R_b^{th}, and the activity resulting from "epicadmium" neutrons, R_b^e.

$$R_b^T = R_b^{th} + R_b^e \qquad (13)$$

Since the true epicadmium neutron produced activity of a cadmium covered foil and bare foil are the same, the true epicadmium activity may be expressed as

$$R_{cd}^e(\text{true}) = R_b^e = F_{cd} \left[R_{cd}^T(\text{obs}) - R_{cd}^{th}(\text{obs}) \right]. \qquad (14)$$

Since

$$R_{cd}^{th}(\text{obs}) = X \, R_b^{th}$$

Eqn (14) can be re-written

$$R_b^e = \left[R_{cd}^T(\text{obs}) - X \, R_b^{th} \right] \, F_{cd}. \qquad (15)$$

In using foils to compare thermal neutron fluxes with similar spectra, the data of prime interest are the count rates of activities that result from thermal neutrons. The saturated activity count rate of a bare foil resulting from thermal neutrons can be expressed:

$$R_b^{th} = R_b^T - R_b^e = R_b^T - \left[R_{cd}^T(\text{obs}) - X \, R_b^{th} \right] \, F_{cd}. \qquad (16)$$

By solving Eqn (16) for R_b^{th} the following expression is obtained

$$R_b^{th} = \frac{R_b^T - F_{cd} \, R_{cd}^T(\text{obs})}{1 - X \, F_{cd}} \qquad (17)$$

This is the expression that is used in place of R_s in Eqn (7) when thermal neutron fluxes are compared that have a spectrum such that the velocity of part of the neutrons is greater than the region of $1/v$ variation in the neutron cross section.

Note that the value of R_b^{th} could have been determined directly from Figure 6 by equating it to the difference between R_b^T and the extrapolated intercept for zero thickness cadmium cover.

III. DESIGN AND DESCRIPTION OF PILE

Graphite has several desirable properties which make it useful in nuclear work. Some of these properties are: availability, machinability, high moderating ratio, good temperature characteristics, low activation cross section, and low cost. The neutron economy, or high moderating ratio, stems from its small capture cross section (3.3 millibarns), and its low atomic weight. Owing to the low atomic weight of carbon a fast neutron will suffer an average loss of about 16 percent of its energy in each scattering event. The density of the graphite is about 1.66 gm/cm^3 and its microscopic scattering cross section is approximately 4.8 barns, hence a neutron will have a scattering mean free path (m.f.p.) of about 2.50 cm in graphite. The ratio of the fractional energy loss by scattering to the m.f.p. is the slowing down power of a moderator. Using the above figures, the slowing down power of graphite is 0.064. The ratio of the slowing down power to the microscopic cross section is called the moderating ratio. This number is used as a figure of merit for moderating materials, and has the value of approximately 170 for graphite. This compares very favorably with all substances except heavy water which has a moderating ratio on the order of 12,000; however, ordinary water has a ratio of only 72. Almost all elements have a greater absorption coefficient than carbon; consequently, impurities in graphite tend to decrease its moderating ratio and thus should be avoided.

A drawing of the pile is shown in Figure 1. Figure 2 is a cutaway drawing indicating how the pile is constructed. The graphite pile is constructed from 4 in. x 4 in. x 50 in. parallelpipeds of reactor grade graphite (AGOT). It consists of 18 crossed layers, each 4 in. thick, 48 in. wide, and 50 in. long. The assembled pile is enclosed by 1/32 in. cadmium which in turn is enclosed by an attractive aluminum honeycombed insulating panel. The cadmium serves the dual purpose of preventing thermal neutrons from escaping from the pile and preventing thermal neutrons external to the pile from entering the pile. Large external sources of fast neutrons will have to be avoided since their presence might invalidate the calibration of the pile. However, insofar as the internal source is concerned, the cadmium assures that the flux inside the pile is relatively independent of the external environment. The word relatively is used here since external materials might scatter escaping fast neutrons back into the graphite lattice. This effect will be so small as to be essentially negligible.

The graphite lattice assembly rests on an aluminum plate 50 in. x 50 in. x 1/2 in., which in turn is supported by a sturdy framework of aluminum "I" beams. The outermost graphite elements in the lattice are secured in position by means of graphite dowling plugs and
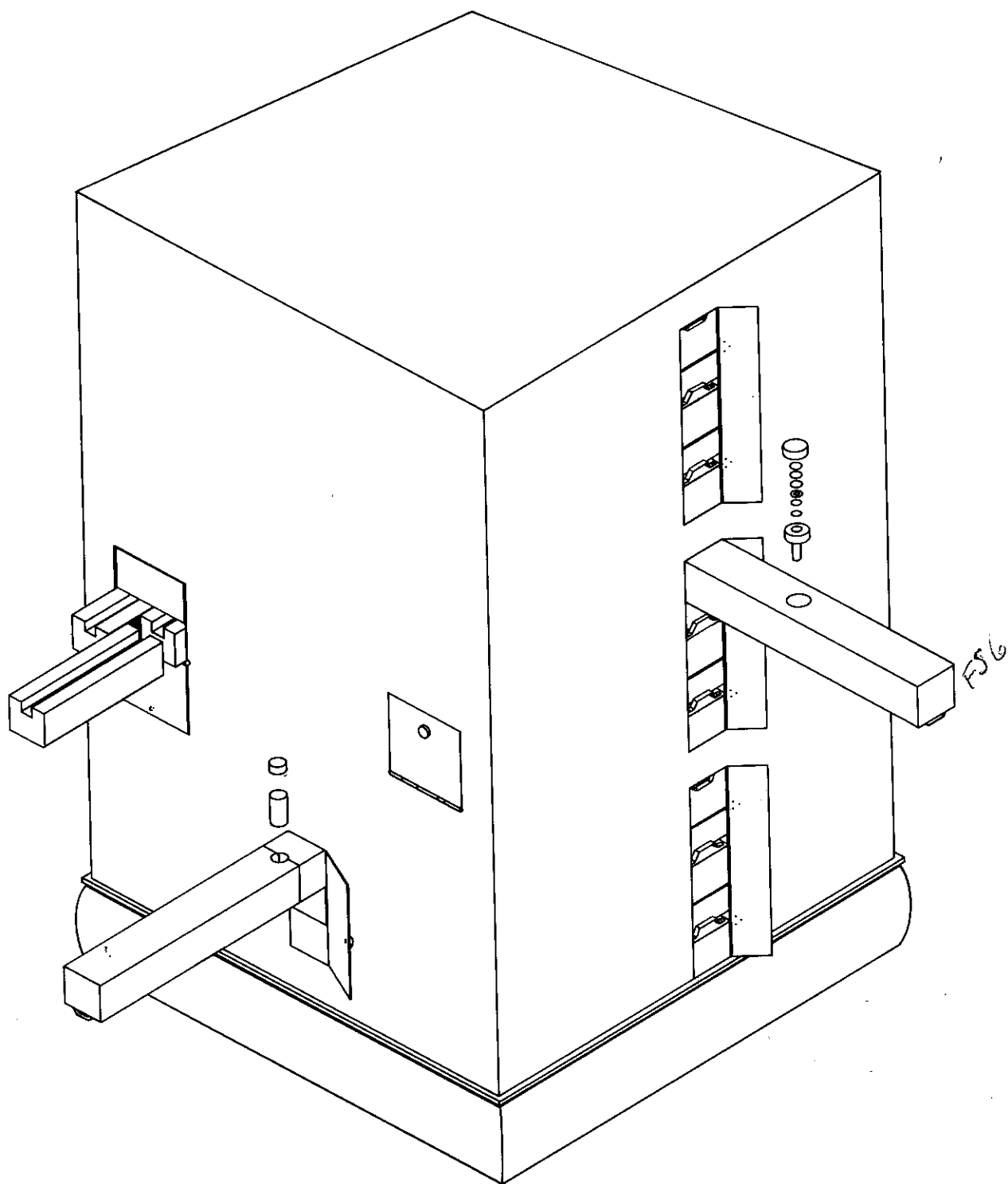
Figure 1. Drawing of Complete Graphite Standard Pile

Figure 2. Cutaway Drawing of Graphite Standard Pile Showing Wooden Supports and Removable Stringers Marked "S"

a maple wood framework which can be seen in Figure 2.

The stringers, those elements which slide in and out of the lattice, are 3.99 in. x 3.99 in. x 50 in. parallelepipeds. The 0.010 in. undersize of these elements allows them to slide in and out of the lattice without affecting the remaining lattice elements. The stringers protrude one inch from the surface of the vertically adjacent lattice elements. They are also provided with small handles so that they may be easily grasped and pulled out of the lattice. Doors are provided at both the back and front ends of the stringers. The accurate position of each stringer is checked visually by assuring that it is flush with the adjacent lattice elements in the horizontal direction. This is indicated in Figure 2 by the "in position" stringers marked with the letter "S."

The foil slots in the nine foil stringers on the front face of the pile are constructed by drilling a 2.500 inch diameter hole to a depth of 1.875 inches with the center 23 inches from the front surface of the stringer as shown in Figure 1 and Figure 3a. A 3/4 inch diameter hole was drilled on center the remaining distance of 2.115 inches through the stringer. The foil plug for the stringer is a split plug. The upper section of the plug is a disc 2.490 inches in diameter and 0.375 inches thick. The lower section of the plug is 3.625 inches long with the bottom 2.125 inch portion being 0.740 inch in diameter and the upper 1.500 inch portion being 2.490 inches in diameter. A hole 1.500 inches in diameter is center bored 0.375 inches deep in this part of the plug to position the foils in the plug. A foil is positioned in this region by means of 1/16 inch thick graphite filler plugs. This permits positioning foils to the closest 1/16 inch distance from the source. Foils with diameters up to 1.500 inches and of thicknesses up to 0.375 inch thick can be accommodated simply by drilling a hole of the desired diameter through the necessary number of 1/16 in. thick graphite filler plugs. Placing a foil in the foil plug is a very simple operation. The plug is removed from the stringer by pushing up on the bottom plug through the hole that is drilled through the stringer. The lower plug is inverted to remove the filler plugs. The foil is placed in the appropriate position in the stack of filler plugs which are then returned to the recess in the lower plug. The lower and upper plugs are then returned to the hole in the foil stringer. Since the length of the plug assembly is slightly greater than the thickness of the foil stringer, the plug will show a slight vertical movement as it moves past the outer surface of the vertically adjacent lattice elements during insertion and removal of a foil stringer.

The source stringer is shown in an exploded view in Figure 3b and withdrawn from the pile in Figure 1. Access to this stringer is provided by front and back doors that can be locked at the
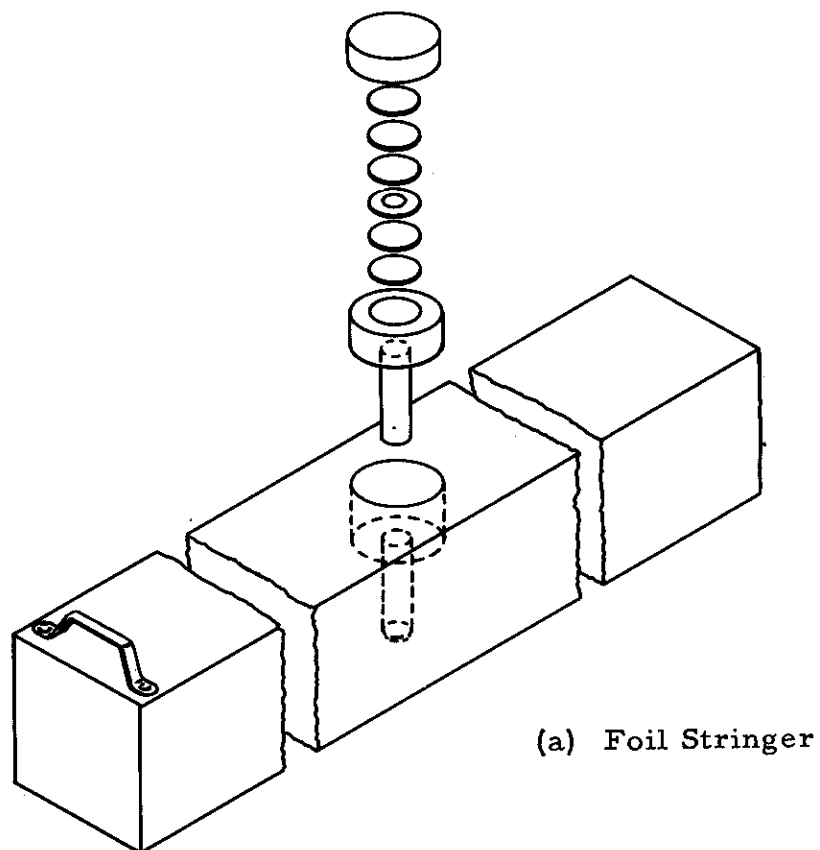
(a) Foil Stringer
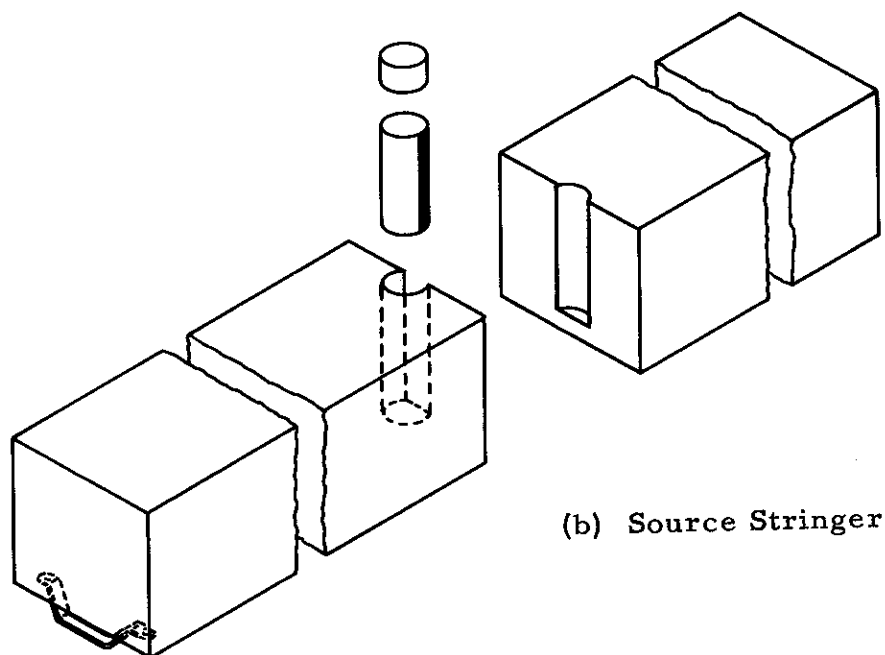
(b) Source Stringer

Figure 3. Detail Drawing of Stringers

discretion of the person in charge of operating the pile. Having these doors locked assures the operator that the source stringer will not be inadvertently moved. This stringer accurately positions the center of the source at a point in the lattice 57.9 in. from the top of the graphite lattice. Actually, the geometrical axis of the lattice is displaced 2.83 inches from the source's central axis. This results from the number and size of the graphite elements employed in each layer, i.e., twelve 4 in. x 4 in. x 50 in. elements per layer as shown in Figure 4.

A beam of fast and thermal neutrons is obtained by viewing the source directly when the back section of the source stringer that does not hold the source is removed. By inserting a cadmium or boron-impregnated sleeve in the 4 in. x 4 in. x 26.600 in. cavity the thermal component of the beam can be eliminated. A neutron spectrum, approximating that shown in Figure 5, can be obtained.

The graphite pile is also provided with two double stringers which permit irradiation of instruments that have a cross sectional area as great as 4 in. x 8 in. These double stringers, as shown in Figure 1, are in the fourth layer of stringers above the source stringer. Access to these stringers is on the same side of the pile as the access to the source stringers. As shown in Figure 2, the double stringers are the second and third stringers from the side of the pile. Both of these stringers making up a double stringer are cut in two pieces with lengths of 23 in. and 27 in. Both the 23 in. section and 27 in. section are provided with handles on the external ends. A groove 0.250 in. deep and 0.500 in. wide is machined in the top surface of each of these stringers to permit running electrical leads or small tubes to the instrument or device being irradiated. When an instrument is positioned in the plane of the source (23 in. from the front edge of the source stringer), the front and back sections of the double stringer are permitted to protrude through the access doors.

The symmetry of the removable stringers is such that four sources can be employed simultaneously, each at a distance of 16 in. from a point of symmetry. The point of symmetry is at the top of the foil plug in the sixth foil stringer from the top of the graphite pile. The four points for locating sources 16 in. from the point of symmetry are:

1. the top of the foil plug in the fourth foil stringer from the top of the pile,
2. the bottom of the source stringer directly below the source, and
3. two points at the intersections of the following planes:
    a. the vertical centerline plane of the foil stringers
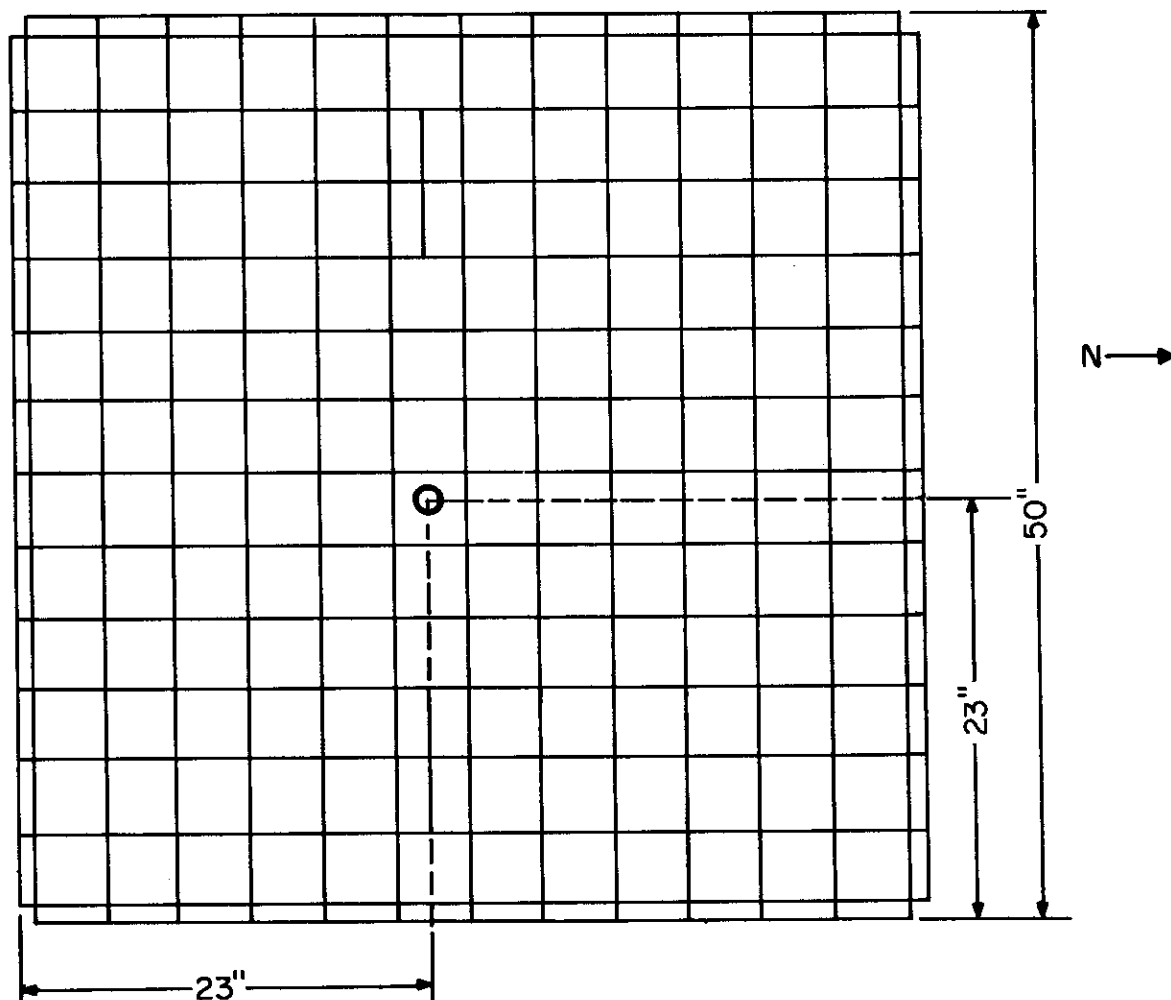
Figure 4.   Top View of Graphite Standard Pile
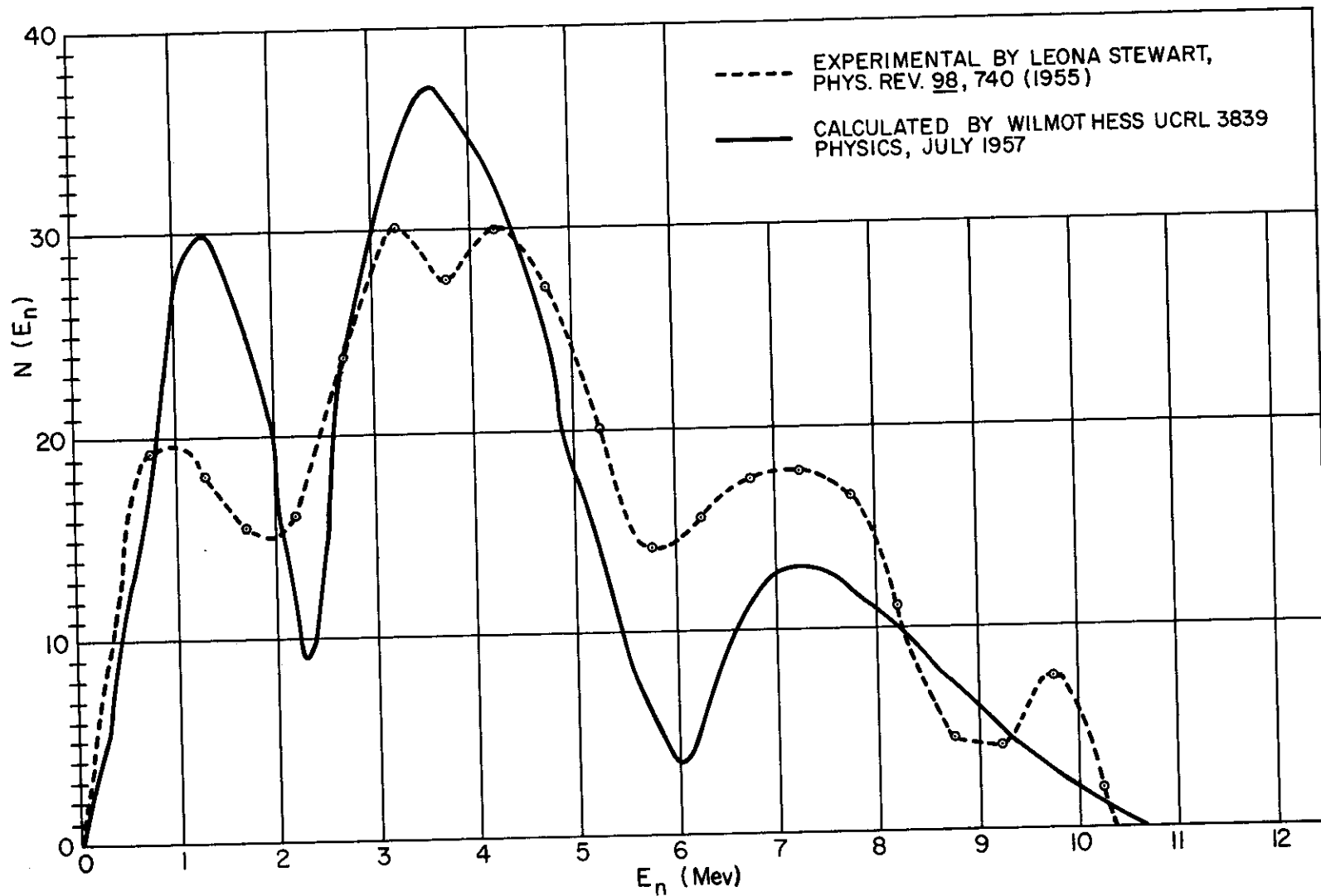
Figure 5. Pu-Be Spectrum

b. the horizontal plane at the bottom of the double
    stringers, and
c. the vertical centerline plane of the fourth stringer
    on each side of the plane of the source stringer.

Since actual sources are not truly point sources but are of finite size,
the readily attainable symmetrical condition is only a good approxima-
tion.

IV. EXPERIMENTAL METHOD AND RESULTS

The absolute value of the thermal neutron flux in the graphite pile was determined by comparison with the thermal neutron standard maintained by the National Bureau of Standards. The NBS thermal neutron standard flux is produced by two one gram Ra-Be (α, n) neutron sources that are permanently fixed in a configuration of lead, paraffin, and graphite. The exposure cavity in the facility is surrounded by graphite. A description of the standard and the method by which it was calibrated was reported by DeJuren and Rosenwasser in 1954. [7] Only one position in the graphite pile was compared directly with the NBS standard. All other positions in the pile were compared with the "standard position."

The irradiation positions in the graphite pile were selected and designated in the following manner. The nine foil positions were designated FS-1 through FS-9 number from the bottom to the top of the pile. The "standard position" is FS-6 which is in the stringer shown to be partially out of the pile in Figure 1. The position in each foil plug is on top of the second 1/16 in. graphite filler wafer. In this position a foil is 3.375 in. above the bottom of the foil plug. The two double stringers (instrument stringers) were designated ISL and ISR, the letters L and R referring to the left and right double stringers as one faces the side of the pile from which the Pu-Be source can be removed. The position calibrated in each of the double stringers was in the vertical plane where the stringers were cut (23 in. from the front edge). It was 2 in. above the bottom of the two stringers and 7/32 in. from the interface of the two stringers towards the outside surface of the pile.

The foils used for the calibration measurements of the "standard position" were goil foils 0.002 in. thick by 0.435 in. diameter. Gold was chosen for these comparison measurements because of its relatively long half life. With the 2.70 day half life, the foils were flown to the Nuclear Experimental Test Facility at Wright Air Development Division in Dayton Ohio where they were counted with the same counting equipment that was later used for other foil measurements in the graphite pile.

The foils used for the comparison of the flux at all other positions in the pile with the flux in the one "standard position" were

---

[7] J. A. DeJuren and H. Rosenwasser, "Absolute Calibration of the NBS Standard Thermal Neutron Density," Journal of Research, National Bureau of Standards, 52, 1954.

high purity indium foils 0.005 in. thick by 7/16 in. diameter. The expected small flux at positions in the pile distant from the source required use of foils that had a large cross section and relatively short half life. This permitted making statistically significant measurements of the induced activity without irradiating the foils for exceedingly long periods.

The cadmium covers used for both the gold and indium foil comparison measurements were 0.020 in. thick. These cadmium covers consisted of a disc cover 0.502 in. diameter and a shallow cup that was made from a disc of the same diameter. During irradiation the covers were secured to the shallow cup with tiny strips of transparent adhesive tape.

The measurements made at NBS for determining the cadmium cover correction factor for the gold foils required using cadmium covers of different thicknesses. These covers were made from 0.500 in. diameter discs that were punched from high purity cadmium which had been rolled into foils 0.0053 in., 0.010 in., and 0.033 in. thick. One of the other cadmium covers was used for 0.020 in. thick cadmium cover measurement.

All the foils were counted in a 2π gas-flow proportional counter using 90 percent argon, 10 percent methane as the counting gas. The stability of the counter was checked periodically with a Tl^{204} source. The stability was excellent and no corrections were needed for fluctuations in instrument sensitivity.

In the calibration of the "standard position" weight matched gold foils were irradiated both bare and cadmium-covered in the NBS standard thermal neutron flux and in the "standard position" in the pile. These data and the saturated activity counting rates for each of the foils are given in the tables. To prevent or minimize flux depression and interference between foils, bare foils were never irradiated along with cadmium covered foils. There were two irradiations at NBS; a reproduction of the test report is shown in Figure 6. Two identical bare gold foils, as previously described, and two Aerojet-General Nucleonics gold foils were in the first irradiation at NBS. When these foils were counted the following day, the AGN foils did not show a statistically significant count rate in the 2π gas flow counter. This should have been expected since these foils have a protective aluminum cover 0.030 in. thick which absorbs most of the Au^{198} betas; they are designed for use with gamma scintillation counting equipment. One of the previously irradiated foils and three other weight matched gold foils with cadmium covers 0.0053 in., 0.010 in., 0.020 in., and 0.033 in. thick were in the second irradiation at NBS. The data obtained from counting the foils from the

UNITED STATES DEPARTMENT OF COMMERCE
NATIONAL BUREAU OF STANDARDS
WASHINGTON 25, D. C.

National Bureau of Standards
Test Report

NBS Test Number 163032
IRRADIATION OF NEUTRON ACTIVATION DETECTORS IN NBS STANDARD
FOR THERMAL NEUTRON FLUX

Detectors submitted by:
American Machine and Foundry Company
1025 North Royal Street
Alexandria, Virginia

Purchase Order No. 8763

IRRADIATION DATA: The activation detectors were mounted onto an
aluminum foil holder and irradiated for the period given below.

Detector Identification	Irradiation Conditions	Date-Time (EST)
Gold Foils: (AGN 380, AGN 381, 18, 22)	Bare	Fr 4:09 PM, 2 August 1960 to 4:00 PM, 4 August 1960
Gold Foils: (16, 19, 21, 22)	in individual cadmium covers	Fr 9:11 AM 25 August 1960 to 3:30 PM 30 August 1960

Foils were irradiated by J. Chin (NBS-4.07). The data is recorded on
p.132 of NBS-RPL data book number 455.

THE STANDARD FLUX: The NBS standard thermal neutron flux is produced
by two one-gram Ra-Be (α,n) sources permanently fixed in a moderating
geometry of paraffin and graphite. The exposure cavity is in graphite.
A boron film calibration of the flux was reported in J. Research NBS 52, 93 (1954)
by J. DeJuren and H. Rosenwasser. A gold foil calibration will be reported
in J. Nuclear Energy by E. R. Mosburg, Jr., and W. M. Murphey. Allowing a
couple percent for undiscovered systematic errors and using the least
standard error estimate of 1 percent, the cadmium difference flux was
4.21 ($\pm$5%)x10^3 neutrons/cm^2-sec. Using Westcott's convention, this is
equivalent to 4.23($\pm$5%)x10^3 neutrons/cm^2-sec.

4.07
Project 04625
September 19, 1960

R. S. Caswell, Chief
Neutron Physics Section

Figure 6. NBS Thermal Flux Report

second irradiation were used for determining the cadmium cover correction factor. Sufficient time elapsed between irradiations making the residual activity negligible.

Figure 7 is a plot of the relative saturated activity counting rate versus cadmium cover thickness. The curve indicates the cadmium cover correction factor, F_{cd}, for a 20 mil thick cadmium cover to be 1.04. This value is in good agreement with the correction factor of about 1.02 which is applied by the Bureau of Standards for cadmium covers 20, 30, and 40 mils thick over gold foils. Using the method outlined by Tittle,[5] the calculated value of F_{cd} is 1.03 for 20 mil cadmium covers over gold foils.

Figure 8 shows the thermal leakage factor for the gold foils that were covered with different thicknesses of cadmium. Even though there is a rather wide statistical variation present in Figure 8, the thermal part of the activity of 20 mil cadmium covered gold foils is less than 0.1 percent of the total. This value is insignificant in comparison to the counting statistics and uncontrollable errors. With the thermal leakage correction factor, X, essentially equal to zero, equation (17) reduces to

$$R_b^{th} = R_b^T - F_{cd} R_{cd}^T (obs)$$

This is the working equation for obtaining the values used for R_s in equation (7) for comparing two fluxes.

The uncertainty in the value of the standard thermal neutron flux at the National Bureau of Standards completely overshadows the statistical errors in counting the activity of the foils and the determination of the various correction factors. The cadmium difference flux that the Bureau quotes is 4.21 (plus or minus 5 percent) x 10^3 neutrons/cm^2-sec and using Westcott's convention,[8] this is 4.23 (plus or minus 5 percent) x 10^3 neutrons/cm^2-sec.

The value of the cadmium difference thermal neutron flux and the cadmium ratio of the "standard position" are calculated from data shown in Table 1. The cadmium ratio is taken simply as the ratio of the saturated activity counting rate of the bare foil, R_b^T, to the corrected saturated activity counting rate of the cadmium covered foil due to epicadmium neutrons, $F_{cd}R_{cd}^T$ (obs).

The flux at all positions in the pile including the "standard position" was determined by use of identically weight-matched indium

---

[8]C. H. Westcott, paper #15/p/202, 2nd United Nations Conference on Peaceful Uses of Atomic Energy, Vol. 16, "Nuclear Data and Reactor Theory," 70, 26 May 1958.
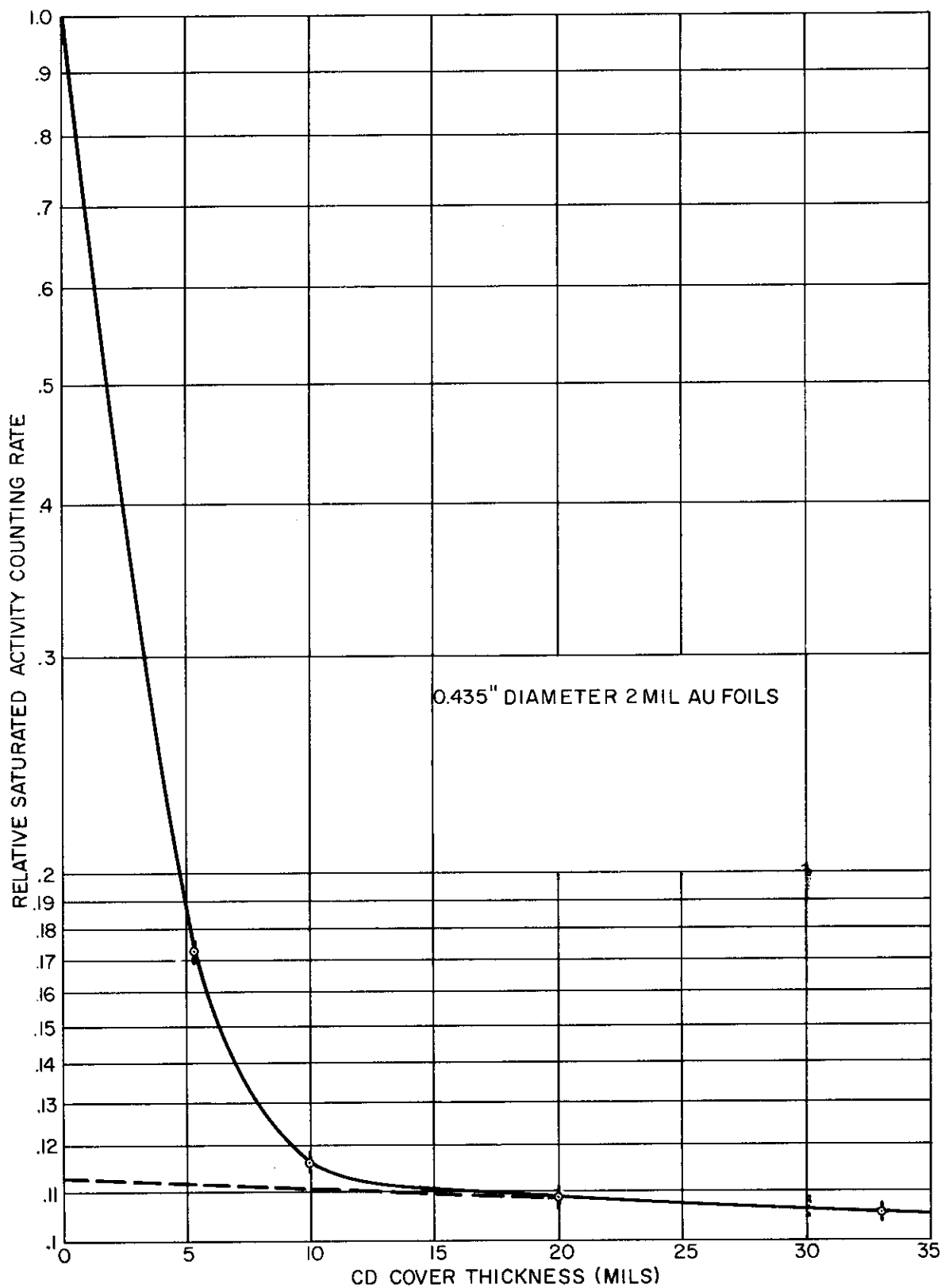
Figure 7. Epicadmium Activity as a Function
of Cadmium Thickness (Measured at NBS)
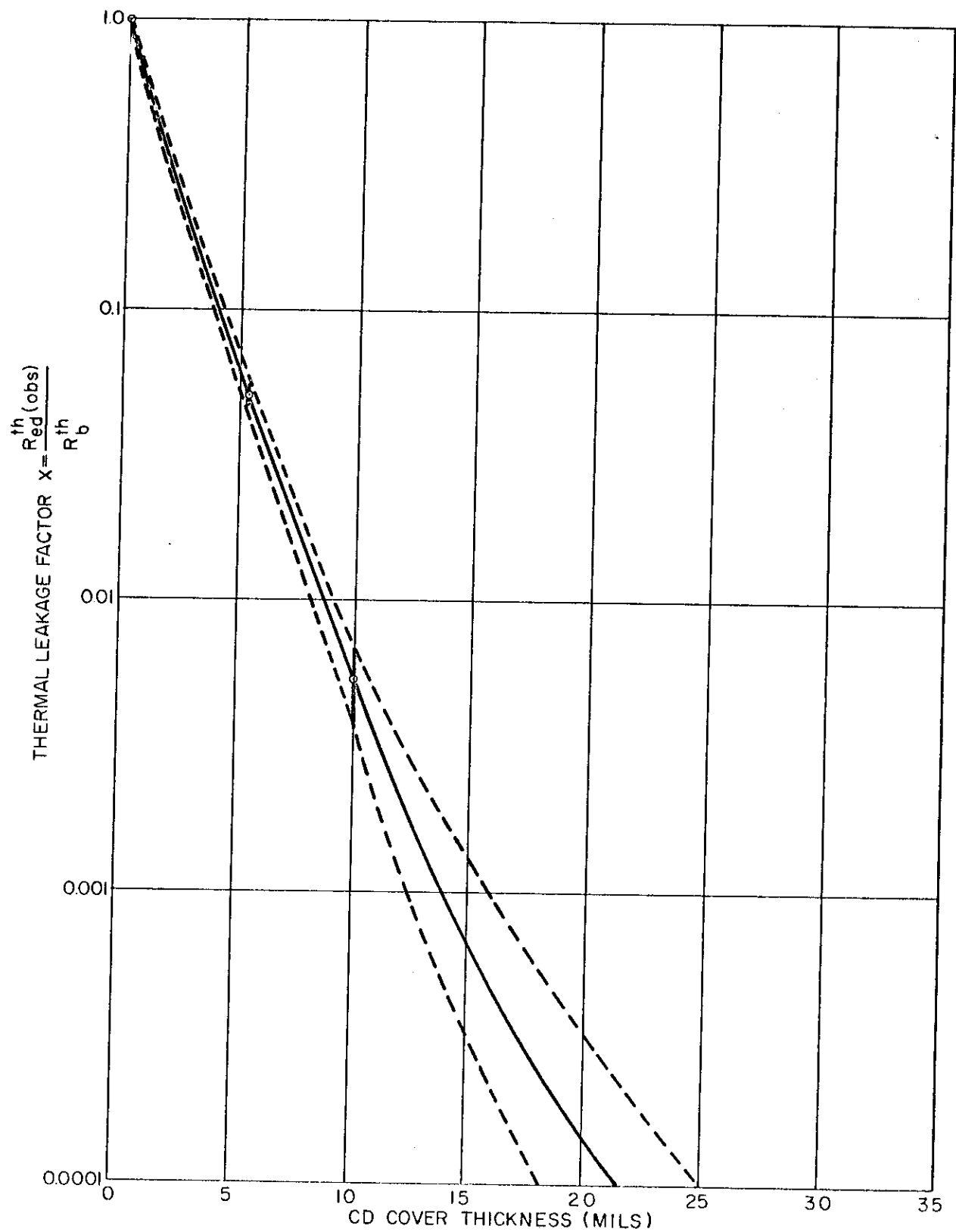
Figure 8. Thermal Leakage Factor for Various Cadmium Thicknesses

Table 1. Results of Gold Foil Irradiations

Gold Foil Number	Foil Weight (gm)	Normalization Factor	Cd Cover Thickness (mils)	Where Irradiated	Irradiation Interval t_e (min)	$\dfrac{1}{1-e^{-\lambda t_e}}$	Wait Interval t_w (min)	$e^{\lambda t_w}$
18	.0944	1.00	Bare	NBS	2,871	2.4963	1298	1.2604
	.0944	1.00	Bare	NBS	2,871	2.4963	1320	1.2654
	.0944	1.00	Bare	NBS	2,871	2.4963	1350	1.2721
22	.0944	1.00	Bare	NBS	2,871	2.4963	1387	1.2806
	.0944	1.00	Bare	NBS	2,871	2.4963	1408	1.2853
18	.0944	1.000	Bare	FS-6	6,925	1.4079	20	1.0036
	.0944	1.000	Bare	FS-6	6,925	1.4079	50	1.0089
	.0944	1.000	Bare	FS-6	6,925	1.4079	80	1.0144
18	.0944	1.000	20	FS-6	10,088	1.1983	160	1.0290
19	.0942	1.0021	5.3	NBS	7,579	1.3493	1430	1.2903
16	.0945	0.9989	10	NBS	7,579	1.3493	1322	1.2657
22	.0944	1.000	20	NBS	7,579	1.3493	1100	1.2165
21	.0945	0.9989	33	NBS	7,579	1.3493	1210	1.2407

Table 1. Results of Gold Foil Irradiations (Continued)

Gold Foil Number	Count Interval t_c (min)	$\dfrac{1}{1-e^{-\lambda t_c}}$	Observed Counts In Interval t_c	Background for Interval t_c	Net Counts for Interval t_c $C(t_c)$	$\dfrac{\lambda C(t_c)\,e^{\lambda t_w}}{(1-e^{-\lambda t_c})(1-e^{-\lambda t_e})}$	
18	20 20 20	285.71 285.71 285.71	10,752 10,499 10,743	1,000 1,000 1,000	9,752 9,499 9,743	1,568 1,534 1,582 Average: 1,561	18 18 18 10
22	20 20	285.71 285.71	10,477 10,613	1,000 1,000	9,477 9,613	1,549 1,577 Average: 1,563	18 18 12
18	30 30 30	188.67 188.67 188.67	12,005 12,094 12,159	1,656 1,656 1,656	10,349 10,347 10,503	493.6 496.2 506.5 Average: 498.8	5.2 5.2 5.3 3
18	1020	6.0096	65,011	55,111	9,900	13.1	.5
19	75	75.19	15,611	4,052	11,559	270.2	2.9
16	100	56.82	15,889	5,403	10,486	181.2	2.2
22	100	56.82	15,640	5,403	10,237	170.1	2.1
21	100	56.82	15,118	5,403	9,715	164.6	2.1

Saturation Rate

foils. Bare foil measurements were taken in all eleven irradiation positions, but measurements with cadmium covered foils were taken in only seven of the positions. The saturated activity counting rate of the cadmium covered foils was plotted against distance from the source, and the saturated activity counting rates at the positions that were not measured were taken from this curve. The measured Cd ratio is plotted in Figure 9 for various distances from the source. The logarithm of the saturated indium resonance flux (corrected cadmium cover) was plotted as a function of the square of the axial distance from the source and is shown in Figure 10. The slope of the portion of the curve was obtained by the method of unweighted least squares to be -0.767×10^{-3} cm^{+2}. Rotating the slope to $-1/4$, the age, τ, was found to be 326 cm^2 which readily agrees with publish - ed values in graphite.[9] Figure 10 also illustrates that the spatial flux distribution not too distant from the source falls off as e^{-kr^2}.

The corrected cadmium difference activity normalized to the absolute thermal neutron flux at the standard position was obtained and is shown in a semilog plot vs. axial distance in Figure 11. As seen from this figure the thermal neutron flux falls off at e^{-kr} at large distances from the source, and the slope yields a relaxation length of 24.2 cm again agreeing with published data.[10] The points near the outer boundaries of the pile break away from the asymptotic value probably because of two effects. One reason for the decrease in the thermal neutron flux may be caused by the finite boundaries in the x and y dimension of the pile, resulting in thermal leakage. The second reason may be a result of the cadmium plate at the pile boun- dary being a sink for thermal neutrons.

No attempt was made experimentally to measure or to calcu- late the thermal flux depression factor, F_{th}, for the same reason that it was not used for the gold foils. The value of the correction factor, F_{cd}, was not experimentally determined, but it was taken from the work by Tittle[5] which gives values of F_{cd} vs. indium foil thickness for different cadmium cover thicknesses. For 0.005 in. thick (88 mg/ cm^2) indium foils, the listed value of F_{cd} is 1.07.

The data that were taken and the saturated activity counting rate for each of the indium foils are given in Table 2. Table 2 gives the data that was used in calculating the cadmium ratio and cad- mium difference flux for each of the irradiation positions. The plot of the cadmium difference flux normalized to absolute thermal neutron flux at the standard position versus distance above and below the geo- metric center of the source is given in Figure 12 and Table 3.

[9] Glasstone, S., and Edlund, M. C., The Element of Nuclear Reactor Theory, D. Van Nostrand Co., Inc., New York, 1952.
[10] Segre, E., Experimental Nuclear Physics, Vol. II, John Wiley & Sons, New York, 1953.
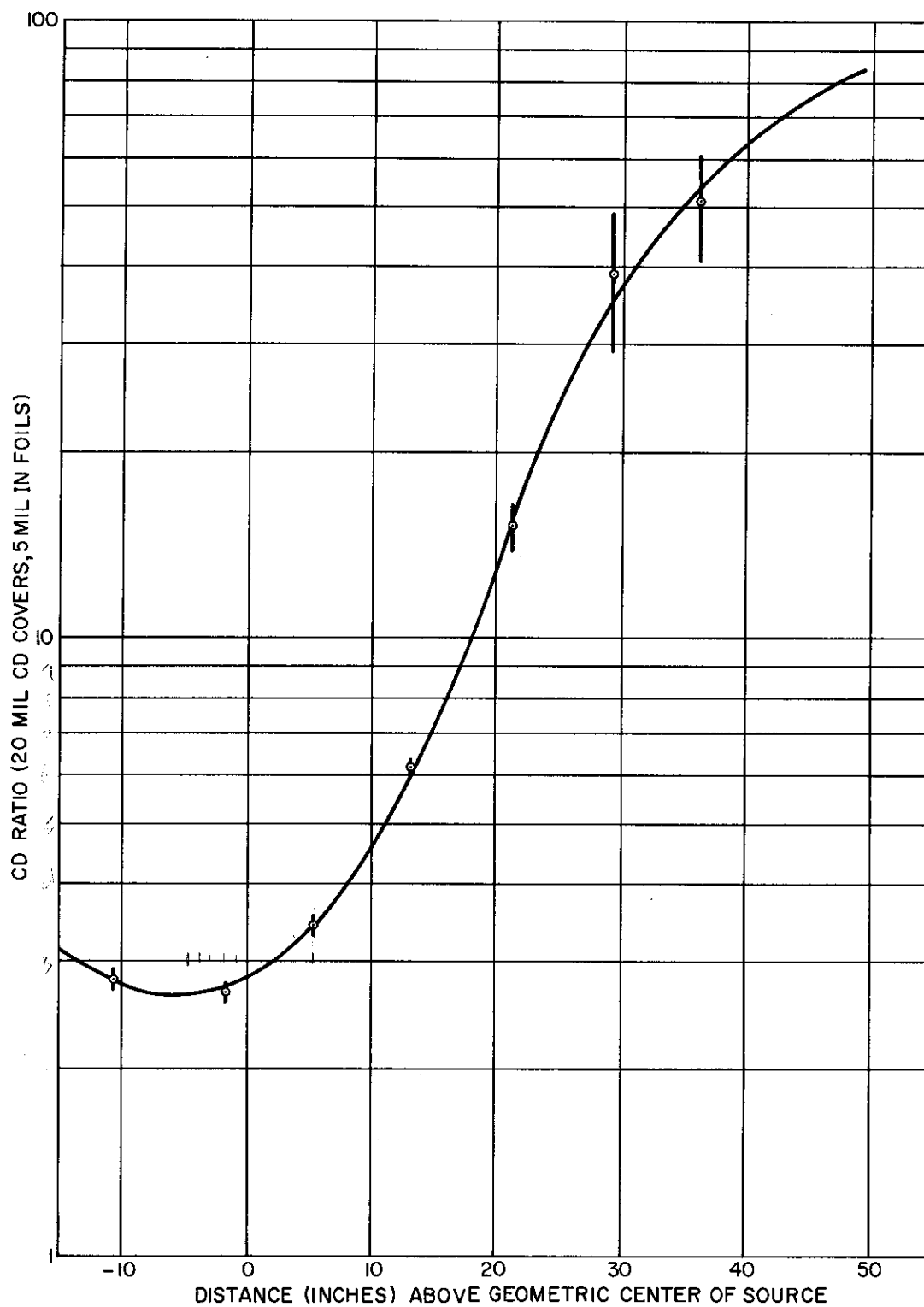
Figure 9. Measured Cadmium Ratio for Various Distances from the Source
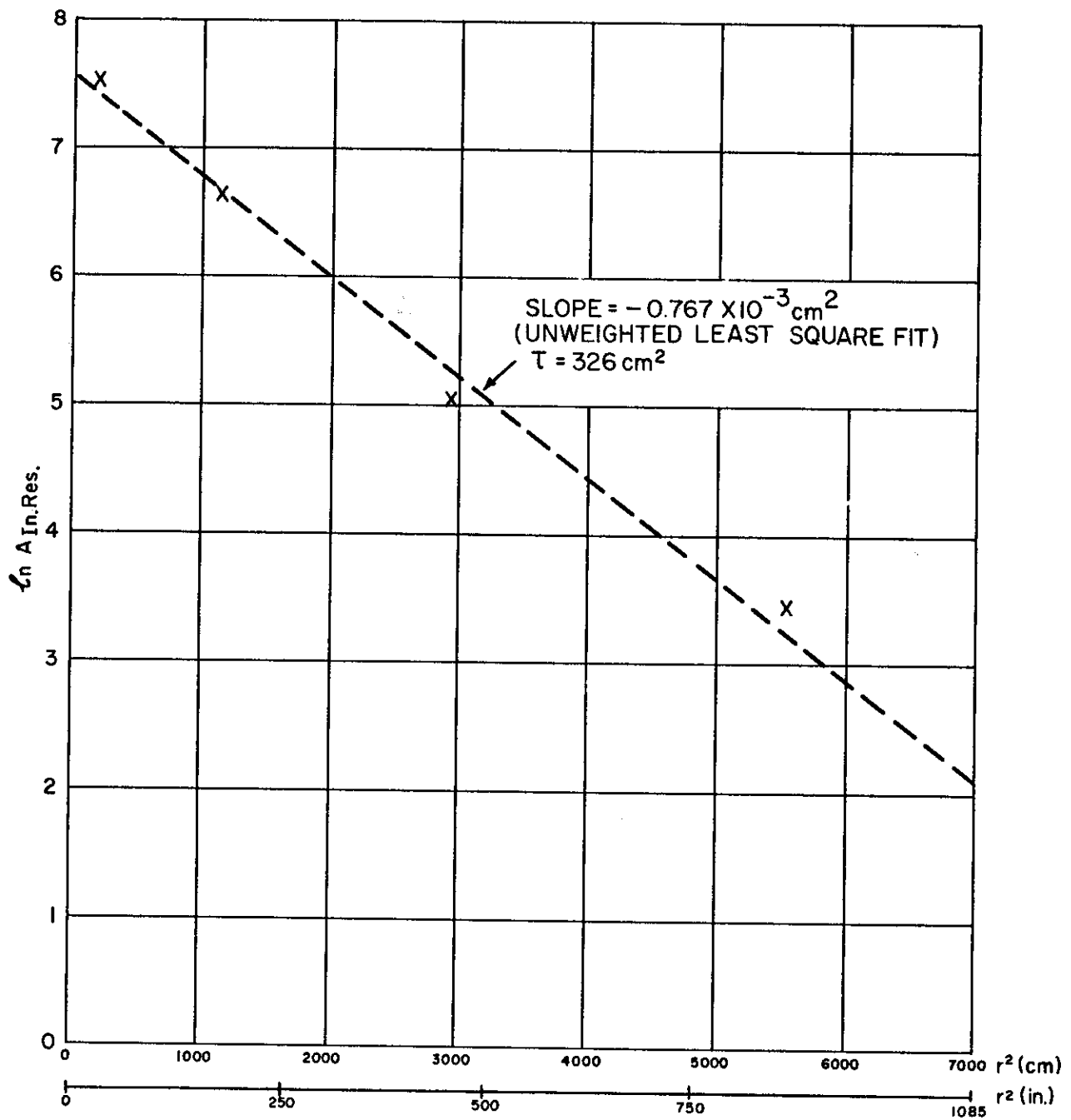
Figure 10. Indium Resonance Activity Versus the Square of Axial Distance from the Source.
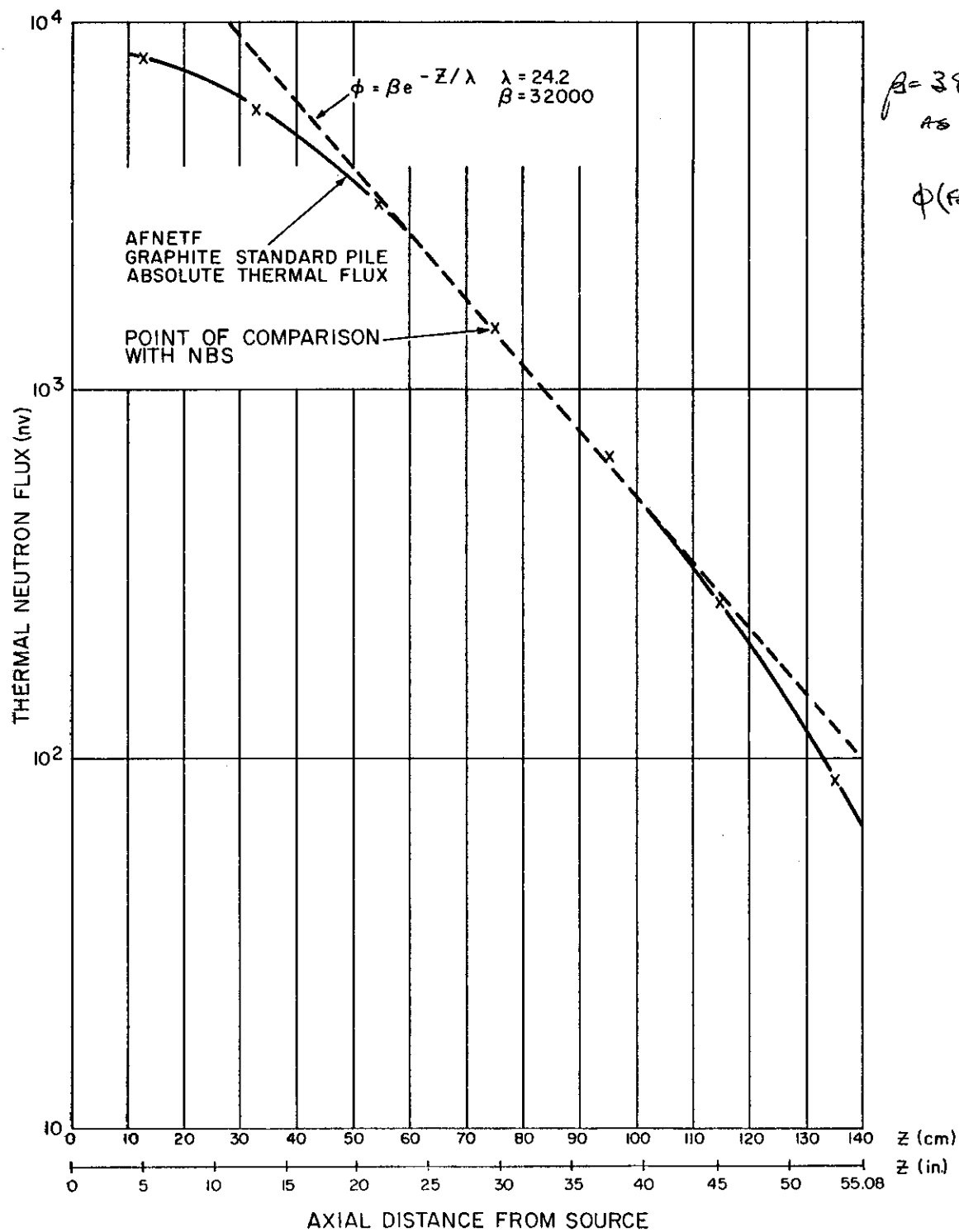
Figure 11. Absolute Thermal Neutron Flux as a Function of the Axial Distance from the Source.

Table 2. Results of Indium Foil Irradiations

Indium Foil	Bare or 20 mil cadmium cover	Irradiation Position	Irradiation Interval T_e (min)	$\dfrac{1}{1-e^{-\lambda t_e}}$	Wait Interval t_w (min)	$e^{\lambda t_w}$	Counting Interval T_c (min)	$\dfrac{1}{1-e^{-\lambda t_c}}$	Observed Counts in Interval t_c	Background for Interval t_c	Net Counts for Interval t_c, $C(t_c)$	$\dfrac{\lambda C(t_c)\,e^{\lambda t_w}}{(1-e^{-\lambda t_e})(1-e^{-\lambda t_c})}$
E	Cd	FS-1	255	1.0394	10	1.1370	15	5.7097	11,061	825	10,236	886.8
B	Cd	FS-3	235	1.0515	10	1.1370	10	8.3012	14,619	550	14,069	1792.7
C	Cd	FS-5	255	1.0394	30	1.4697	40	2.4902	16,727	2200	14,527	709.4
A	Cd	FS-4	180	1.1101	15	1.2123	45	2.2786	6,305	2475	3,830	150.8
D	Cd	FS-6	1235	1.0000	10	1.1370	40	2.4902	3,009	2200	809	29.4
H	Cd	FS-8	1360	1.0000	15	1.2123	60	1.8616	3,540	3300	240	7.0
C	Cd	ISL	1280	1.0000	15	1.2123	60	1.8616	6,162	3300	2,862	82.9
A	Bare	FS-1	285	1.0264	32	1.5082	10	8.3012	21,921	550	21,371	3515.6
H	Bare	FS-2	1190	1.0000	15	1.2123	5	16.086	30,851	275	30,576	7632.2
J	Bare	FS-3	204	1.0786	37	1.6082	10	8.3012	29,271	550	28,721	5292.6
B	Bare	FS-4	1155	1.0000	35	1.5674	3	26.472	15,610	165	15,445	8202.9
I	Bare	FS-5	1270	1.0000	45	1.7821	15	5.7097	21,404	825	20,579	2689.3
C	Bare	FS-6	280	1.0282	15	1.2123	15	5.7097	13,920	825	13,095	1196.7
K	Bare	FS-7	1200	1.0000	15	1.2123	30	3.1289	12,399	1650	10,749	523.5
D	Bare	FS-8	345	1.0121	15	1.2123	60	1.8616	10,719	3300	7,419	217.6
F	Bare	FS-9	1437	1.0000	15	1.2123	120	1.2726	10,112	6600	3,512	71.1
E	Bare	ISR	200	1.0831	13	1.1816	15	5.7097	21,473	825	20,648	1931.3
G	Bare	ISL	1302	1.0000	10	1.1370	15	5.7097	20,753	825	19,928	1656.0
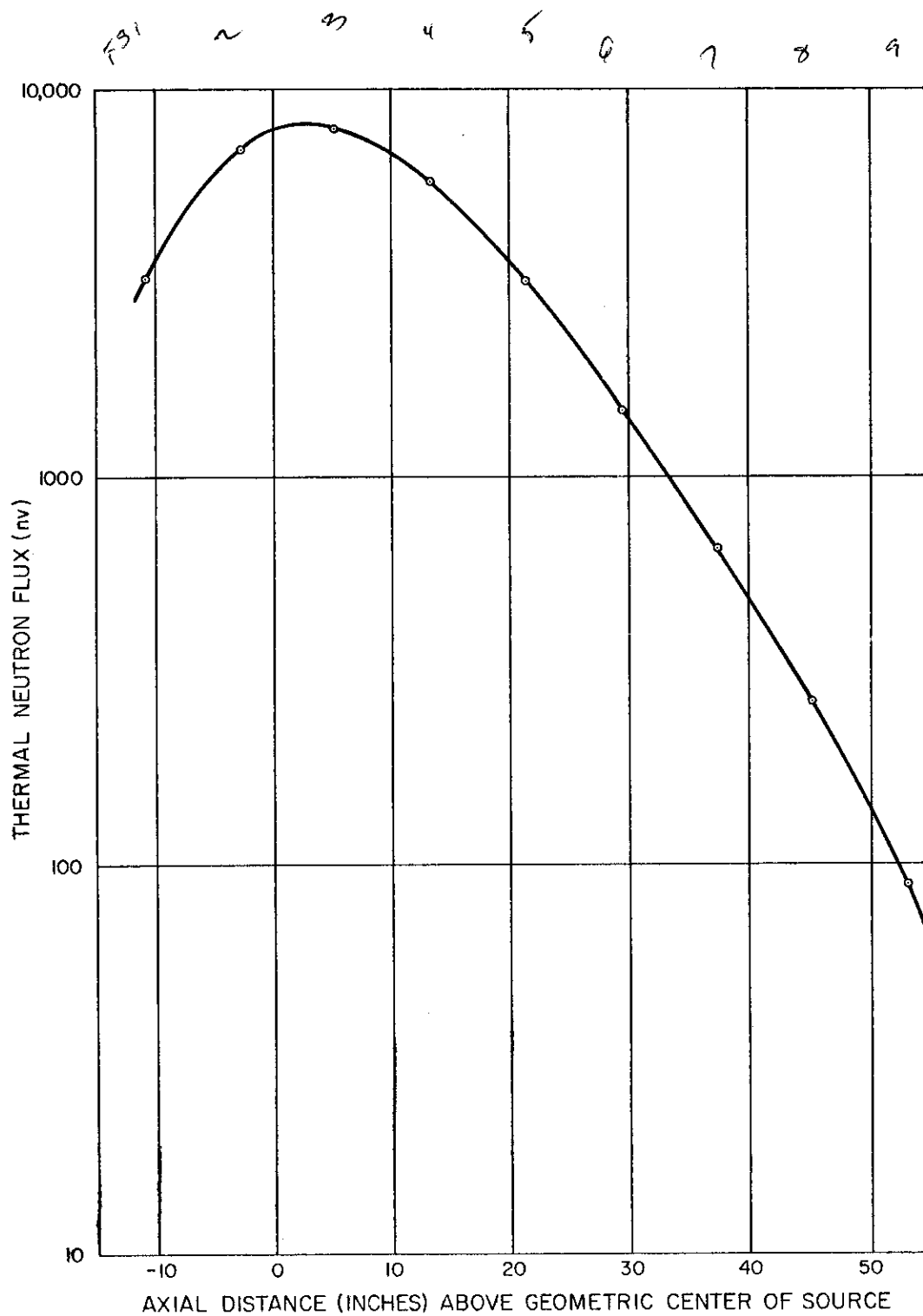
Figure 12. Absolute Thermal Neutron Flux Measured at Various Distances from the Source.

Table 3

Cadmium Difference Flux for Each Foil Position

Foil Position	Cadmium Difference Flux (n/cm^2 sec)	
FS 1	3230	3844
FS 2	6920*	8235
FS 3	7920	9425
FS 4	5720	6807
FS 5	3180	3754
FS 6	1470	1749
FS 7	647*	770
FS 8	265	
FS 9	87*	
ISL	1980	
ISR	2260*	

handwritten: 1.19 x reported

handwritten: Mark Rossano's calculated flux using Am-241 ingrowth (p. 97 of his thesis)

*interpolated points from Figures 9 and 10.

APPENDIX I

EXACT SOLUTION OF AGE-DIFFUSION EQUATION

The experimental data plotted in Figures 8 and 9 show that the flux falls off as e^{-kr^2} near the source and e^{-kr} at greater distances from the source. The following, an exact solution to the age-diffusion equation, is here presented to show that these experimental results are in agreement with theory. The spatial distribution of the thermal neutron density may be computed from this solution using the applicable parameters.

The procedure used was to obtain the appropriate solution of the equation

$$\nabla^2 N(\vec{r}, u_t) - \frac{N(\vec{r}, u_t)}{L^2} = - \frac{\ell_o}{L^2} \; Q(\vec{r}, \tau) \qquad (1)$$

Here N is the thermal neutron density, L is the diffusion length, ℓ_o is the average lifetime of the thermal neutrons in the medium, and $Q(\vec{r}, \tau)$ is the slowing down density. In equation (1), $Q(\vec{r}, \tau)$ is derived from the solution of the Fermi age equation

$$\frac{\partial Q(\vec{r}, \tau)}{\partial \tau} = \nabla^2 Q(\vec{r}, \tau) + \mathcal{S}(\vec{r}, \tau) \qquad (2a)$$

where the source term is assumed separable in space and lethargy so that the distribution of source neutrons is given by

$$\mathcal{S}(\vec{r}, \tau) = S(\vec{r}) \; U(\tau).$$

Equation (2a) now becomes

$$\frac{\partial Q(\vec{r}, \tau)}{\partial \tau} = \nabla^2 Q(\vec{r}, \tau) + S(\vec{r}) \; U(\tau). \qquad (2b)$$

We shall now operate on equation (2b) for boundary conditions on a parallelepiped.

$$0 \leq x \leq a$$

$$0 \leq y \leq b$$

$$N = 0 \text{ at } x = a, \; 0$$
$$N = 0 \text{ at } y = b, \; 0$$

$$N = \frac{\partial N}{\partial z} = 0 \text{ at } z = \pm \infty$$

$$\frac{\partial N}{\partial x} = \frac{\partial N}{\partial y} = \frac{\partial N}{\partial z} = 0 \text{ at } \left(\frac{a}{2}, \frac{b}{2}, 0 \right)$$

To put these equations in an appropriate form to apply a Fourier transform, equation (2b) is multiplied by

$$e^{i\xi z} \sin\left(\frac{m\pi x}{a}\right) \sin\left(\frac{n\pi y}{b}\right),$$

and integrated over the region of the parallelepiped:

$$\int_{-\infty}^{+\infty}\int_{0}^{b}\int_{0}^{a} e^{i\xi z} \sin\left(\frac{m\pi x}{a}\right) \sin\left(\frac{n\pi y}{b}\right) \frac{\partial Q}{\partial \tau} \; dx \; dy \; dz \equiv$$

$$\int_{-\infty}^{+\infty}\int_{0}^{b}\int_{0}^{a} e^{i\xi z} \sin\left(\frac{m\pi x}{a}\right) \sin\left(\frac{n\pi y}{b}\right)\left(\nabla^2 Q + S(\vec{r})\, U\,(\tau)\right) dx \; dy \; dz \quad (3)$$

Examining the first term of expression (3) and expanding the Laplacian we have:

$$\int_{-\infty}^{+\infty}\int_{0}^{b}\int_{0}^{a} e^{i\xi z} \sin\left(\frac{m\pi x}{a}\right) \sin\left(\frac{n\pi y}{a}\right)\; (\nabla^2 Q)\; dx \; dy \; dz \equiv \qquad (4)$$

$$\int_{-\infty}^{+\infty}\int_{0}^{b} f(y,\, z,\, \tau)\; dy \; dz \int_{0}^{a} \sin\left(\frac{m\pi x}{a}\right)\left(\frac{\partial}{\partial x}\; \frac{\partial Q}{\partial x} + \frac{\partial}{\partial y}\; \frac{\partial Q}{\partial y} + \right.$$

$$\left. \frac{\partial}{\partial z}\; \frac{\partial Q}{\partial z}\right) dx. \qquad (4a)$$

Separating this into its component parts, we show that expressions (4) and (4a) are equivalent to

$$\int_{-\infty}^{+\infty}\int_{0}^{b}\int_{0}^{a} e^{i\xi z} \sin\left(\frac{m\pi x}{a}\right)\; \sin\left(\frac{n\pi y}{b}\right)\; \frac{\partial^2 Q}{\partial x^2}\; dx \; dy \; dz$$

$$\int_{-\infty}^{+\infty}\int_{0}^{b}\int_{0}^{a} e^{i\xi z} \sin\left(\frac{m\pi x}{a}\right)\; \sin\left(\frac{n\pi y}{b}\right)\; \frac{\partial^2 Q}{\partial y^2}\; dx \; dz \; dy$$

$$\int_{-\infty}^{+\infty}\int_{0}^{b}\int_{0}^{a} e^{i\xi z} \sin\left(\frac{m\pi x}{a}\right)\; \sin\left(\frac{n\pi y}{b}\right)\; \frac{\partial^2 Q}{\partial z^2}\; dx \; dy \; dz. \qquad (5)$$

We now integrate the first term of (5) by parts:

$$\int_o^a \sin\left(\frac{m\pi x}{a}\right) \frac{\partial^2 Q}{\partial x^2} \, dx = \int_o^a \sin\left(\frac{m\pi x}{a}\right) \frac{\partial}{\partial x} \frac{\partial Q}{\partial x} \, dx$$

Letting $u = \sin\left(\frac{m\pi x}{a}\right)$ and $dv = \frac{\partial}{\partial x} \frac{\partial Q}{\partial x}$

so that $du = \frac{m\pi}{a} \cos\left(\frac{m\pi x}{a}\right) \, dx$ and $v = \frac{\partial Q}{\partial x}$,

we have $\int u\,dv = uv - \int v\,du$

or

$$\int_o^a \sin\left(\frac{m\pi x}{a}\right)\frac{\partial^2 Q}{\partial x^2} \, dx = \frac{\partial Q}{\partial x} \sin\left(\frac{m\pi x}{a}\right)\Big|_o^a - \frac{m\pi}{a} \int_o^a \frac{\partial Q}{\partial x} \cos\left(\frac{m\pi x}{a}\right) dx.$$

$$(6)$$

Since $\sin\left(\frac{m\pi(a)}{a}\right) = \sin\left(\frac{m\pi(0)}{a}\right) = 0$ the first term on the right-hand side

of (6) will drop out in the evaluation from zero to a.

To integrate the second term of (6), we let

$u = \cos\left(\frac{m\pi x}{a}\right)$ and $dv = \frac{\partial Q}{\partial x}$ so that

$du = -\frac{m\pi}{a} \sin\left(\frac{m\pi x}{a}\right) \, dx$ and $v = Q.$

Again integrating by parts:

$$\int_o^a \sin\left(\frac{m\pi x}{a}\right) \frac{\partial^2 Q}{\partial x^2} \, dx = -\frac{m\pi}{a}\left[\cos\left(\frac{m\pi x}{a}\right) Q\Big|_o^a + \frac{m\pi}{a}\int_o^a Q \sin\left(\frac{m\pi x}{a}\right) dx.\right](7)$$

The first term on the right of (7) is zero because of the boundary condition that $\frac{\partial Q}{\partial x} = Q = 0$ at $x = 0$ and $x = a$. Equation (7) then becomes

$$\int_o^a \sin\left(\frac{m\pi x}{a}\right) \frac{\partial^2 Q}{\partial x^2} \, dx = -\left(\frac{m\pi}{a}\right)^2 \int_o^a Q \sin\left(\frac{m\pi x}{a}\right) dx.$$

$$(8)$$

Equation (8) is the required integrated form for the first term of equation (5).

The second term of equation (5) is given by

$$\int_o^b \sin(\frac{n\pi y}{b}) \frac{\partial^2 Q}{\partial y^2} \, dy \quad \text{(including only the y-dependent portion)}.$$

This is the same in form as the first term of equation (5), so a derivation identical to that of (8) will yield

$$\int_o^b \sin(\frac{n\pi y}{b}) \frac{\partial^2 Q}{\partial y^2} \, dy = -(\frac{n\pi}{b})^2 \int_o^b Q \sin \frac{n\pi y}{b} \, dy. \qquad (9)$$

We will now consider the third term of equation (5). The expression

$$\int_{-\infty}^{+\infty} e^{i\xi z} \frac{\partial^2 Q}{\partial z^2} \, dz \quad \text{will be integrated by parts.} \quad \text{We let}$$

$$u = e^{i\xi z} \text{ and } dv = \frac{\partial^2 Q}{\partial y^2} \text{ so that}$$

$$du = i\xi e^{i\xi z} \text{ and } v = \frac{\partial Q}{\partial z}.$$

We then have

$$\int_{-\infty}^{+\infty} e^{i\xi z} \frac{\partial^2 Q}{\partial z^2} \, dz = \frac{\partial Q}{\partial z} e^{i\xi z} \Big|_{-\infty}^{+\infty} - i\xi \int_{-\infty}^{+\infty} \frac{\partial Q}{\partial z} e^{i\xi z} \, dz. \qquad (10)$$

Then $\frac{1}{2} (e^{i\xi z} + e^{-i\xi z}) = \cos \xi z$ or $e^{i\xi 3} = 2 \cos \xi z - e^{-i\xi z}$,

and $\frac{1}{2i} (e^{i\xi z} - e^{-i\xi z}) = \sin \xi z$ or $e^{-i\xi z} = e^{i\xi z} - 2i \sin \xi z.$

Combining,

$$e^{i\xi z} = 2 \cos \xi z + 2i \sin \xi z - e^{i\xi z} \quad \text{or}$$

$$e^{i\xi z} = \cos \xi z + i \sin \xi z, \qquad (11)$$

and it is seen that $e^{i\xi z} < i \infty$ everywhere.

As z approaches $+\infty$ the neutron flux ϕ has a form given by

$$\phi(z) = A e^{-Bz} \text{ so that } \frac{\partial \phi}{\partial z} = -ABe^{-Bz}.$$

then $\lim\limits_{z\to\infty} \dfrac{\partial\phi}{\partial z} = \lim\limits_{z\to-\infty} \dfrac{\partial\phi}{\partial z} = 0.$

Since $Q \cong \xi \Sigma_t \phi,$

$$\frac{\partial Q}{\partial z} = \xi\Sigma_t \quad \frac{\partial Q}{\partial z} = 0 \text{ as } z \to \pm\infty.$$

Then the first term on the right of equation (10) is zero, and (10) becomes

$$\int_{-\infty}^{+\infty} e^{i\xi z} \frac{\partial^2 Q}{\partial z^2} \, dz = -i\xi \int_{-\infty}^{+\infty} \frac{\partial Q}{\partial z} \, e^{i\xi z} \, dz. \tag{12}$$

We let $u = e^{i\xi z}$ and $dv = \dfrac{\partial Q}{\partial z}$ so that $du = i\xi \, e^{i\xi z} \, dz$ and $v = Q$, and integrate (12) to obtain

$$\int_{-\infty}^{+\infty} e^{i\xi z} \frac{\partial^2 Q}{\partial z^2} \, dz = -i\xi \left[\Big[Q e^{i\xi z} \Big]_{-\infty}^{+\infty} -i\xi \int Q e^{i\xi z} \, dz \right]$$

as above, $Q e^{i\xi z} \Big[_{-\infty}^{+\infty} = 0$ since $Q = 0$ at $z = \pm\infty,$ so we have

$$\int_{-\infty}^{+\infty} e^{i\xi z} \frac{\partial^2 Q}{\partial z^2} \, dz = -\xi^2 \int_{-\infty}^{+\infty} Q e^{i\xi z} \, dz. \tag{13}$$

Equation (13) is the required integrated form for the third term of equation (5). We then substitute expressions (8), (9), and (13) into (5) to obtain

$$\int_{-\infty}^{+\infty}\int_{0}^{b}\int_{0}^{a} (-\frac{m\pi}{a})^2 \, e^{i\xi z} \sin\left(\frac{m\pi x}{a}\right) \sin\left(\frac{n\pi y}{b}\right) Q \, dx \, dy \, dz$$

$$+ \int_{-\infty}^{+\infty}\int_{0}^{b}\int_{0}^{a} -(\frac{n\pi}{b})^2 \, e^{i\xi z} \sin\left(\frac{m\pi x}{a}\right) \sin\left(\frac{n\pi y}{b}\right) Q \, dx \, dy \, dz$$

$$+ \int_{-\infty}^{+\infty}\int_{0}^{b}\int_{0}^{a} -\xi^2 \, e^{i\xi z} \sin\left(\frac{m\pi x}{a}\right) \sin\left(\frac{n\pi y}{b}\right) Q \, dx \, dy \, dz. \tag{14}$$

Expression (14) is then substituted into (3), yielding:

$$\int_{-\infty}^{+\infty}\int_0^b\int_0^a e^{i\xi z}\,\sin\left(\frac{m\pi x}{a}\right)\sin\left(\frac{n\pi y}{b}\right)\frac{\partial Q}{\partial \tau}\,dx\,dy\,dz =$$

$$\int_{-\infty}^{+\infty}\int_0^b\int_0^a e^{i\xi z}\,\sin\left(\frac{m\pi x}{a}\right)\sin\left(\frac{n\pi y}{b}\right)Q\left[(-\xi^2-\left(\frac{m\pi}{a}\right)^2-\left(\frac{n\pi}{b}\right)^2 +\right.$$

$$\left.\frac{S(\vec{r})\,U(\tau)}{Q(\vec{r},\tau)}\right]\,dx\,dy\,dz. \tag{15}$$

We now define

$$\bar{q}\,(\xi,\ m,\ n)\equiv\frac{1}{\sqrt{2\pi}}\int_{-\infty}^{+\infty}\int_0^b\int_0^a Qe^{i\xi z}\sin\left(\frac{m\pi x}{a}\right)\sin\left(\frac{n\pi y}{b}\right)\,dx\,dy\,dz \tag{16}$$

and

$$\bar{s}\,(\xi,\ m,\ n)\equiv\frac{1}{\sqrt{2\pi}}\int_{-\infty}^{+\infty}\int_0^b\int_0^a Se^{i\xi z}\sin\left(\frac{m\pi x}{a}\right)\sin\left(\frac{n\pi y}{b}\right)\,dx\,dy\,dz. \tag{17}$$

Since, generally,

$$\int f(x)\,\frac{\partial F(x,\tau)}{\partial \tau}\,dx = \frac{\partial}{\partial \tau}\int f(x)\,F(x,\tau)\,dx,$$

equation (15) can be written, changing the left-hand side:

$$\frac{\partial}{\partial \tau}\int_{-\infty}^{+\infty}\int_0^b\int_0^a e^{i\xi z}\,\sin\left(\frac{m\pi x}{a}\right)\sin\left(\frac{n\pi y}{b}\right)Q\,dx\,dy\,dz =$$

$$\int_{-\infty}^{+\infty}\int_0^b\int_0^a e^{i\xi z}\,\sin\left(\frac{m\pi x}{a}\right)\sin\left(\frac{n\pi y}{b}\right)Q\left[-\xi^2-\left(\frac{m\pi}{a}\right)^2-\left(\frac{n\pi}{b}\right)^2+\frac{SU}{Q}\right]$$

$$dx\,dy\,dz. \tag{18}$$

We then substitute (16) and (17) into (18), obtaining

$$\frac{\partial}{\partial \tau}\left(\sqrt{2\pi}\ \bar{q}\ (\xi, m, n)\right) = \sqrt{2\pi}\ \bar{q}\left[-\xi^2 - (\frac{m\pi}{a})^2 - (\frac{n\pi}{b})^2\right] + \sqrt{2\pi}\ \bar{S}\ (\xi, m, n)\ U, \quad (19)$$

and, dividing by $\sqrt{2\pi}$,

$$\frac{\partial \bar{q}}{\partial \tau} = \bar{q}\left[-\xi^2 - (\frac{m\pi}{a})^2 - (\frac{n\pi}{b})^2\right] + \bar{S}\left[U\right]. \quad (20)$$

Equation (20) is of the form $\frac{dy}{dx} - ay = f(x)$, where the integrating factor I is given by

$$I = \exp\left(\int_{\tau_o}^{\tau}\left[\xi^2 + (\frac{m\pi}{a})^2 + (\frac{n\pi}{b})^2\right]dt\right)$$

$$= \exp\left[\xi^2 + (\frac{m\pi}{a})^2 + (\frac{n\pi}{b})^2\right]\ \left[\tau - \tau_o\right]. \quad (21)$$

Solving (20) for $\bar{q}$, and employing I from (21), we have

$$\bar{q} = \frac{A}{I} + \frac{\bar{S}}{I}\int_{\tau_o}^{\tau} I\ (t)\ U\ (t)\ dt \quad (22)$$

where A is an arbitrary constant of integration. We now expand a function of Q in a Fourier series, letting

$$\frac{ab}{4\sqrt{2\pi}}\int_{-\infty}^{+\infty} Q\ (x, y, z)\ e^{i\xi z}\ dz \cong \sum_{n=1}^{\infty} \sum_{m=1}^{\infty} d_{mn}\ \sin\frac{m\pi x}{a}\sin\frac{n\pi y}{b}. \quad (23)$$

Here the constant d_{mn} is determined in the usual manner by multiplying both sides by the factor sin px sin qy and then integrating over x and y. The result is

$$d_{mn} = \frac{4}{\pi^2}\int_{s=0}^{\pi}\int_{t=0}^{\pi}\int_{z=-\infty}^{+\infty} Q\ (s, t, z)\ e^{i\xi z}\left[\frac{ab}{4\sqrt{2\pi}}\right]\sin(ms)\sin(nt)\ dz\ dt\ ds. \quad (24)$$

We then let $s = \frac{\pi x}{a}$ and $t = \frac{\pi y}{b}$, so that $ds = \frac{\pi}{a}\ dx$ and $dt = \frac{\pi}{b}\ dy$. Then

$$d_{mn} = \frac{4}{\pi^2}\left[\frac{ab}{4\sqrt{2\pi}}\right]\int_{-\infty}^{+\infty}\int_{0}^{b}\int_{0}^{a} Q\ (x, y, z)\ e^{i\xi z}\sin(\frac{m\pi x}{a})\sin(\frac{n\pi y}{b})\ \frac{\pi}{a}\ dx\ \frac{\pi}{b}$$

$$dy\ dz \quad (25)$$

or, re-written,

$$d_{mn} = \frac{1}{\sqrt{2\pi}} \int\limits_{-\infty}^{+\infty} \int\limits_{0}^{b} \int\limits_{0}^{a} Q(x,y,z) e^{i\xi z} \sin\left(\frac{m\pi x}{a}\right) \sin\left(\frac{n\pi y}{b}\right) dx\, dy\, dz. \quad (26)$$

Then equation (27) corresponds to (16); $d_{mn} = \bar{q}(\xi, m, n)$, and:

$$q(\xi, m, n) = \frac{1}{\sqrt{2\pi}} \int\limits_{-\infty}^{+\infty} \int\limits_{0}^{b} \int\limits_{0}^{a} Q(x,y,z) e^{i\xi z} \sin\left(\frac{m\pi x}{a}\right) \sin\left(\frac{n\pi y}{b}\right) dx\, dy\, dz. \quad (27)$$

Rearranging, we obtain:

$$\frac{1}{\sqrt{2\pi}} \int\limits_{-\infty}^{+\infty} Q(x,y,z) e^{i\xi z}\, dz \cong \frac{4}{ab} \sum_{n=1}^{\infty} \sum_{m=1}^{\infty} \sin\left(\frac{m\pi x}{a}\right) \sin\left(\frac{n\pi y}{b}\right) \overline{q}(\xi, m, n) \quad (28)$$

Equation (28) is of the form $d(\xi) = \frac{1}{2\pi} \int\limits_{-\infty}^{+\infty} f(z)\, e^{i\xi z}\, dz,$

which has the Fourier transform

$$f(z) = \frac{1}{\sqrt{2\pi}} \int\limits_{-\infty}^{\infty} d(\xi) e^{i\xi z}\, d\xi.$$

We transform (28) to obtain:

$$Q(x,y,z) = \frac{1}{\sqrt{2\pi}} \int\limits_{-\infty}^{\infty} \left[\frac{4}{ab} \sum_{n=1}^{\infty} \sum_{m=1}^{\infty} \sin\left(\frac{m\pi x}{a}\right) \sin\left(\frac{n\pi y}{b}\right) \overline{q}(\xi, m, n) \right] e^{iz\xi}\, d\xi, \quad (29)$$

where $d(u)$ corresponds to the right side of (28) and $f(t)$ corresponds to $Q(x,y,z)$. We now substitute (22) into (29) to obtain

$$Q(x,y,z,\tau) = \frac{1}{\sqrt{2\pi}} \quad e^{iz\xi} \frac{4}{ab} \sum_{n=1}^{\infty} \sum_{m=1}^{\infty} \sin\left(\frac{m\pi x}{a}\right) \sin\left(\frac{n\pi y}{b}\right)$$

$$\left\{ \frac{A}{I} + \frac{\overline{S}}{I} \int\limits_{\tau_0}^{\tau} I(t)\, U(t)\, dt \right\}\, d\xi. \quad (30)$$

Equation (30) is the solution to equation (2). By applying an appropriate boundary condition to $Q(x, y, z, \tau)$ the constant A can be determined.

We now consider again equation (1):

$$\nabla^2 N(\vec{r}, \tau_t) - \frac{N(r, \tau_t)}{L^2} = \frac{\ell_0}{L^2} Q(\vec{r}, \tau_t) \tag{1}$$

As before, we multiply (1) by $e^{i\xi z} \sin\frac{m\pi x}{a} \sin\frac{n\pi y}{b}$ and integrate over the parallelepiped region to obtain:

$$\int_{x=0}^{a}\int_{y=0}^{b}\int_{z=-\infty}^{\infty} e^{i\xi z} \sin\frac{m\pi x}{a} \sin\frac{n\pi y}{b} \left[\nabla^2 N(x, y, z, \tau_t) - \frac{N(x, y, z)}{L^2} \right]$$

$$dx\, dy\, dz = -\frac{\ell_0}{L^2}\int_{x=0}^{a}\int_{y=0}^{b}\int_{z=-\infty}^{\infty} e^{i\xi z} \sin\frac{m\pi x}{a} \sin\frac{n\pi y}{b} Q(x, y, z, \tau_t)\, dx\,dy\,dz \tag{31}$$

The left side of (31) is similar to the right side of equation (3) in form, and by proceeding through the processes of equations (4) through (15) we obtain:

$$-\frac{\ell_0}{L^2} \int_{x=0}^{a}\int_{y=0}^{b}\int_{z=-\infty}^{\infty} e^{i\xi z} \sin\frac{m\pi x}{a} \sin\frac{n\pi y}{b} Q(x, y, z, \tau_t)\, dx\, dy\, dz =$$

$$\int_{x=0}^{a}\int_{y=0}^{b}\int_{z=-\infty}^{\infty} e^{i\xi z} \sin\frac{m\pi x}{a} \sin\frac{n\pi y}{b} N(x, y, z, \tau_t) \left[-\xi^2 - \left(\frac{m\pi}{a}\right)^2 - \right.$$

$$\left. \left(\frac{n\pi}{b}\right)^2 - \frac{1}{L^2} \right] dx\, dy\, dz \tag{32}$$

Now we expand $\dfrac{ab}{4\sqrt{2\pi}} \displaystyle\int_{z=-\infty}^{\infty} N(x, y, z, \tau_t)\, e^{i\xi z}\, dz$ in a Fourier series, letting:

$$\frac{ab}{4\sqrt{2\pi}} \int_{-\infty}^{\infty} N(x, y, z, \tau_t)\, e^{i\xi z}\, dz \cong \sum_{n=1}^{\infty}\sum_{m=1}^{\infty} e_{mn} \sin\frac{m\pi x}{a} \sin\frac{n\pi y}{b} \tag{33}$$

Then, as in (26), the constant e_{mn} can be found by:

$$e_{mn} = \frac{1}{\sqrt{2\pi}} \int_{x=0}^{a}\int_{y=0}^{b}\int_{z=-\infty}^{\infty} N(x, y, z, \tau_t)\, e^{i\xi z} \sin\frac{m\pi x}{a} \sin\frac{n\pi y}{b}\, dx\, dy\, dz. \tag{34}$$

We define $e_{mn} \equiv N(\xi, m, n) = \dfrac{1}{\sqrt{2\pi}} \displaystyle\int_{x=0}^{a} \int_{y=0}^{b} \int_{z=-\infty}^{\infty} N(x, y, z, \tau_t) \, e^{i\xi z} \sin\dfrac{m\pi x}{a}$

$$\sin\dfrac{n\pi y}{b} \ dx \ dy \ dz \tag{35}$$

and substitute (35) and (27) into (32) to obtain:

$$-\dfrac{2\sqrt{\pi}\,l_o}{L^2} \ \ \overline{q}(\xi, m, n) = \left[-\xi^2 - \left(\dfrac{m\pi}{a}\right)^2 - \left(\dfrac{n\pi}{y}\right)^2 - \dfrac{1}{L^2}\right]\sqrt{2\pi} \ \ \overline{N}. \tag{36}$$

Dividing by $-\sqrt{2\pi}$, (36) becomes

$$\dfrac{l_o}{L^2} \ \ \overline{q}(\xi, m, n) = \left[\xi^2 + \left(\dfrac{m\pi}{a}\right)^2 + \left(\dfrac{n\pi}{b}\right)^2 + \dfrac{1}{L^2}\right]\overline{N}(\xi, m, n) \tag{37}$$

and solving for $\overline{N}$, we obtain

$$\overline{N}(\xi, m, n) = \dfrac{l_o}{L^2\left[\xi^2 + \left(\dfrac{m\pi}{a}\right)^2 + \left(\dfrac{n\pi}{b}\right)^2 + \dfrac{1}{L^2}\right]} \ \overline{q}(\xi, m, n). \tag{38}$$

We write (33) as

$$\dfrac{1}{\sqrt{2\pi}}\int_{-\infty}^{\infty} N(x, y, z) \, e^{i\xi z} \ dz = \sum_{n=1}^{\infty}\sum_{m=1}^{\infty} \left[\dfrac{4}{ab} \ e_{mn}\right] \sin\dfrac{m\pi x}{a} \sin\dfrac{n\pi y}{b} \tag{39}$$

which, like (28), has the form $d(\xi) = \dfrac{1}{\sqrt{2\pi}}\displaystyle\int_{-\infty}^{\infty} f(z) \, e^{i\xi z} \ dz,$

with $d(\xi)$ representing the entire right side of (39). Taking the transform of (39), we obtain

$$N(x, y, z, \tau_t) = \dfrac{1}{\sqrt{2\pi}}\int_{-\infty}^{\infty}\sum_{n=1}^{\infty}\sum_{m=1}^{\infty}\dfrac{4}{ab} \ \overline{N}(\xi, m, n, \tau_t) \sin\dfrac{m\pi x}{a} \sin\dfrac{n\pi y}{b}$$

$$e^{iz\xi} \ d\xi. \tag{40}$$

Substituting (38) into (40) and taking all functions not a function of ξ out of the integral yields:

$$N(x, y, z, \tau_t) = \dfrac{4 l_o}{\sqrt{2\pi} \ ab \ L^2} \ \sum_{m=1}^{\infty}\sum_{n=1}^{\infty} \sin\dfrac{m\pi y}{a} \sin\dfrac{n\pi y}{b}$$

$$\int_{z=-\infty}^{\infty} \dfrac{\overline{q}(\xi, m, n, \tau_t) \, e^{iz\xi}}{\left[\xi^2 + \left(\dfrac{m\pi}{a}\right)^2 + \left(\dfrac{n\pi}{b}\right)^2 + \dfrac{1}{L^2}\right]} \tag{41}$$

Substitution of (22) into the integral portion of (41), with $\tau = \tau_t$, will provide the complete solution for N.

We examine the integral of (41):

$$\int_{-\infty}^{\infty} f(\xi, m, n, \tau_t)\, d\xi = \int_{\xi=-\infty}^{\infty} \frac{\dfrac{A}{I} + \dfrac{\overline{S}}{I} \displaystyle\int_{\tau_o}^{\tau_t} I(t)\, U(t)\, dt}{[\,\xi^2 + (\frac{m\pi}{a})^2 + (\frac{n\pi}{b})^2 + \frac{1}{L^2}\,]}\, e^{iz\xi}\, d\xi \quad (42)$$

or, rewriting:

$$\frac{\overline{S}}{I} \int_{\tau_o}^{\tau_t} I(t)\, U(t)\, dt = \overline{S}\, e^{-\int_{\tau_o}^{\tau_t} a\, dt'} \int_{\tau_o}^{\tau_t} e^{\int_{\tau_o}^{\tau_t} a\, dt} U(t)\, dt \quad (43)$$

where $a = [(\frac{m\pi}{a})^2 + (\frac{n\pi}{b})^2 + \xi^2\,]$.

Further,

$$\frac{\overline{S}}{I} \int_{\tau_o}^{\tau_t} I(t)\, U(t)\, dt = \overline{S}\, e^{-a[\tau_t - \tau_o]} \int_{\tau_o}^{\tau_t} e^{a[\tau - \tau_o]} U(t)\, dt$$

$$= \overline{S} \int_{\tau_o}^{\tau_t} e^{a[t - \tau_o + \tau_o - \tau_t]} U(t)\, dt = \overline{S} \int_{\tau_o}^{\tau_t} U(t)\, e^{[(\frac{m\pi}{a})^2 + (\frac{n\pi}{b})^2 + \xi^2](t - \tau_t)}\, dt \quad (44)$$

Substituting (44) into (42) gives:

$$\int_{-\infty}^{\infty} f(\xi, m, n, \tau)\, d\xi =$$

$$\int_{-\infty}^{\infty} \frac{Ae^{-[\xi^2 + (\frac{m\pi}{a})^2 + (\frac{n\pi}{b})^2](\tau_t - \tau_o)} + \overline{S} \displaystyle\int_{\tau_o}^{\tau_t} U(t) e^{[(\frac{m\pi}{a})^2 + (\frac{n\pi}{b})^2 + \xi^2](t - \tau_t)}\, dt}{[\,\xi^2 + (\frac{m\pi}{a})^2 + (\frac{n\pi}{b})^2 + \frac{1}{L^2}\,]}\, d\xi. \quad (45)$$

In the pile, the source $S(x, y, t, \tau) = S(x, y, z)\, U(\tau)$ is zero everywhere except at the coordinate point of the source (x_o, y_o, z_o). Therefore we let

$$S(x, y, z) = S(x_o, y_o, z_o)\, \delta(x - x_o,\ y - y_o,\ z - z_o) \quad (46)$$

where δ is the Dirac delta function, and x_o, y_o, z_o are the coordinates of the point source.

Then (17) becomes:

$$\overline{S}(\xi, m, n) = \frac{1}{\sqrt{2\pi}} \int_x \int_y \int_z S(x_0, y_0, z_0)\, e^{i\xi t} \sin\frac{m\pi x}{a}\ \sin\frac{n\pi y}{b} \delta(x-x_0, y-y_0, z-z_0)$$
$$dx\ dy\ dz, \qquad (46)$$

and, making use of the Delta function property

$$\int_{x-\epsilon}^{x+\epsilon} F(x)\, \delta(x-x_0)\, dx \equiv F(x),$$

$$\overline{S}(\xi, m, n) = \frac{1}{\sqrt{2\pi}} S(x_0, y_0, z_0)\, e^{i\xi z_0} \sin\frac{m\pi x_0}{a} \sin\frac{n\pi y_0}{b}. \qquad (47)$$

Equation (47) can now be substituted into (45) to obtain

$$\int\!\!\int_{\xi=-\infty}^{\infty} \left[\frac{A e^{-\left[\xi^2 + (\frac{m\pi}{a})^2\ (\frac{n\pi}{b})^2\right]\left[\tau - \tau_0\right]}}{\left[\xi^2 + (\frac{m\pi}{a})^2 + (\frac{n\pi}{b})^2 + \frac{1}{L^2}\right]} \right. +$$

$$\left. \frac{\frac{1}{\sqrt{2\pi}} S(x_0, y_0, z_0)\ e^{i\xi z_0}\ \sin\frac{n\pi x_0}{a}\ \sin\frac{n\pi y_0}{b} \int_{\tau_0}^{\tau_t} U(t)\, e^{\left[a'(t-\tau_t)dt\right]}}{\left[\xi^2 + (\frac{m\pi}{a})^2\ (\frac{n\pi}{b})^2 + \frac{1}{L^2}\right]} \right] d\xi. \qquad (48)$$

Equation (48) represents the farthest point that we can reach in the solution of (41) for N (x, y, z, τ) until some knowledge of the function U(τ), the source spectrum, is obtained. In addition, the constant of integration A must be determined from an appropriate boundary condition. The Pu-Be source spectrum ranges from 0 to 10 Mev with peaks at about 1 Mev, 4 Mev, and 7 Mev, and a minor peak at about 9.7 Mev. It falls to zero above 10 Mev. Therefore, we will choose lethargy U = 0 at E = 10 Mev, which causes τ to be zero at that energy. One boundary condition is that N (x, y, z, τ=0) = 0, (independent of x, y, z). From Equation (41), all expressions before the integral over ξ do not necessarily take on a null value as $\tau \to 0$, so the term under the integral must be zero at $\tau = 0$. Hence we have:

$$\lim_{\tau \to 0} \int_{-\infty}^{\infty} \frac{\frac{A}{I} + \frac{\overline{S}}{I} \int_{\tau_0}^{\tau} I(t)\, U(t)\, dt}{\xi^2 + (\frac{m\pi}{a})^2\ (\frac{n\pi}{b})^2 + \frac{1}{L^2}}\ e^{i\xi z}\, d\xi = 0. \qquad (49)$$

Here τ_0 is an arbitrary value of τ chosen for the integrating factor of (21). Now we will choose $\tau_0 = 0$, which forces the integral over the

dummy variable t in (49) to be zero, and we have:

$$\lim_{\tau \to 0} \int_{-\infty}^{\infty} \frac{A}{I\left[\xi^2 + (\frac{m\pi}{a})^2 + (\frac{n\pi}{b})^2 + \frac{1}{I^2}\right]} e^{iz\xi}\, d\xi = 0 . \tag{50}$$

From (21) we have $I = e^{\int_{\tau_0}^{\tau}\left[\xi^2 + (\frac{m\pi}{a})^2 + (\frac{n\pi}{b})^2\right]\, dt}$

and thus $\lim_{\tau \to 0} I = e^0 = 1$ when $\tau_0 \equiv 0$. Then, setting $I = 1$ in the denominator of (50) we get:

$$\lim_{\tau \to 0} \int_{-\infty}^{\infty} \frac{A e^{i\xi z}\, d\xi}{\left[\xi^2 + (\frac{m\pi}{a})^2 + (\frac{n\pi}{b})^2 + \frac{1}{L^2}\right]} = 0 . \tag{51}$$

Since nothing in (51) is a function of τ, A must be zero, and (22) becomes

$$\overline{q}(\xi, m, n, \tau) = \frac{\overline{S}}{I}\int_0^{\tau} I(t)\, U(t)\, dt . \tag{52}$$

Also, (30) becomes, for the solution of $Q(x, y, z, \tau)$,

$$Q(x, y, z, \tau) = \frac{1}{\sqrt{2\pi}} \int_{-\infty}^{\infty} e^{iz\xi} \left[\frac{4}{ab} \sum_{n=1}^{\infty} \sum_{m=1}^{\infty} \sin\frac{m\pi x}{a} \sin\frac{n\pi y}{b} \right.$$

$$\left. \left\{ \frac{\overline{S}}{I} \int_0^{\tau} I(t)\, U(t)\, dt \right\} \right] d\xi . \tag{53}$$

Note that $\lim_{\tau \to 0} Q(x, y, z, \tau) = 0$ also, as it goes as the integral over t in (53), equalling zero when $\tau = 0$.

Eq.(48) (used to solve Eq.(41) for $N(x, y, z, \tau)$) now becomes:

$$(45) = \int_{-\infty}^{\infty} \frac{S(x_0, y_0, z_0)\, e^{iz_0\xi} \sin\frac{m\pi x_0}{a} \sin\frac{n\pi y_0}{b}}{\left[\xi^2 + (\frac{m\pi}{a})^2 + (\frac{n\pi}{b})^2 + \frac{1}{L^2}\right]} \left[\int_0^{\tau_t} U(t) e^{\left[\xi^2 + (\frac{m\pi}{a})^2 (\frac{n\pi}{b})^2\right](t-\tau_t)}\, dt\right] d\xi . \tag{54}$$

Returning to U (t), we assume, as a first approximation, that U (t) = U (t) $\delta(t-t_0)$. (55)

This is a monoenergetic source distribution whose energy E is at E_0, corresponding to τ_0, $0 < \tau_0 < \tau_t$.
Then:

$$\int_0^{\tau_t} U(t) e^{\left[\xi^2 + \left(\frac{m\pi}{a}\right)^2 + \left(\frac{n\pi}{b}\right)^2\right](t-\tau_0)} \delta(t-t_0) \, dt =$$

$$U(\tau_0) \, e^{\left[\xi^2 + \left(\frac{m\pi}{a}\right)^2 + \left(\frac{n\pi}{b}\right)^2\right](\tau_0 \tau_t)}$$

and expression (45) becomes:

$$\int_{-\infty}^{\infty} \frac{S(x_0, y_0, z_0) \, e^{iz_0\xi} \sin \frac{m\pi x_0}{a} \sin \frac{n\pi y_0}{b}}{\left[\xi^2 + \left(\frac{m\pi}{a}\right)^2 + \left(\frac{n\pi}{b}\right)^2 + \frac{1}{L^2}\right]}$$

$$\left(U(\tau_0) \, e^{\left[\xi^2 + \left(\frac{m\pi}{a}\right)^2 + \left(\frac{n\pi}{b}\right)^2\right](\tau_0 - \tau_t)} \right) d\xi. \qquad (56)$$

Collecting all terms not a function of ξ, we have for (45):

$$S(x_0, y_0, z_0) \, U(\tau_0) \sin \frac{m\pi x_0}{a} \sin \frac{n\pi y_0}{b} e^{\left[\left(\frac{m\pi}{a}\right)^2 + \left(\frac{n\pi}{b}\right)^2\right](\tau_0 \tau_t)}$$

$$\int_{-\infty}^{\infty} \frac{e^{iz\xi + \xi^2(\tau_0 \tau_t)}}{\left[\xi^2 + \left(\frac{m\pi}{a}\right)^2 + \left(\frac{n\pi}{b}\right)^2 + \frac{1}{L^2}\right]} \, d\xi \qquad (57)$$

Inserting (57) into (41) provides the solution

$$N(x, y, z, \tau_t) = \frac{4\ell_o}{\sqrt{2\pi}\ ab\ L^2} \sum_{n=1}^{\infty} \sum_{m=1}^{\infty} \sin\left\{ \frac{m\pi x}{a} \sin\frac{n\pi y}{b}\sin\frac{m\pi x}{a}_o \sin\frac{n\pi y_o}{b}\right\}$$

$$\left\{ S(x_o, y_o, z_o)\ U(\tau_o)e^{[(\frac{m\pi}{a})^2(\frac{n\pi}{b})^2](\tau_o - \tau_t)}\right\}\ F(z)$$

where
$$F(z) \equiv \int_{-\infty}^{\infty} \frac{e^{iz\xi + \xi^2(\tau_o - \tau_t)}\ d\xi}{[\xi^2 + (\frac{m\pi}{a})^2 + (\frac{n\pi}{b})^2 + \frac{1}{L^2}]}$$

We must now put this expression for $F(z)$ into a form from which it may be evaluated and used.

If $f(x)$ is a reasonable function we have

$$f(x) = \sqrt{\frac{2}{\pi}} \int_o^{\infty} d\lambda\ F(\lambda)\ \cos\ (\lambda x)$$
$$\text{and}\quad F(\lambda) = \sqrt{\frac{2}{\pi}} \int_o^{\infty} dx\ f(x)\ \cos\ (\lambda x).$$

We consider

$$A = \int_o^{\infty} d\lambda\ F(\lambda)\ G(\lambda)\ \cos\ (\lambda x).$$

It can be seen that

$$A = \int_o^{\infty} d\lambda\ F(\lambda)\ G(\lambda)\ \cos\ (\lambda x) = \int_o^{\infty} d\lambda\ F(\lambda)\ \sqrt{\frac{2}{\pi}}\int_o^{\infty} dy\ g(y)\ \cos\ (\lambda y)\ \cos\ (\lambda x)$$

$$= \frac{1}{2}\int_o^{\infty} dy\ g(y)\ \sqrt{\frac{2}{\pi}}\int_o^{\infty} d\lambda\ F(\lambda)\ \left\{\cos\ \lambda\ (x-y) + \cos\ \lambda\ (x+y)\right\}\ .$$

We can then invert the notation provided $(x-y) > 0$, and obtain:

$$A = \frac{1}{2}\int_o^{\infty} dy\ g(y)\ f(|x-y|)\ + \frac{1}{2}\int_o^{\infty} dy\ g(y)\ f(x+y)$$

Setting $\mu = \tau_o - \tau_t$ and $\beta^2 = (\frac{m\pi}{a})^2 + (\frac{n\pi}{b})^2 + \frac{1}{L^2}$,

we have

$$\int_{-\infty}^{\infty} \frac{d\xi \ e^{-\xi^2\mu} \ e^{-iz\xi}}{(\xi^2 + \beta^2)} = \int_{-\infty}^{\infty} \frac{d\xi \ e^{-\xi^2\mu}}{\xi^2 + \beta^2} \{\cos z\xi - i \sin z\xi\}$$

$$= 2 \int_{0}^{\infty} \frac{d\xi \ e^{-\mu\xi^2}}{\xi^2 + \beta^2} \cos(\xi z) \ ,$$

where $\displaystyle\int_{-\infty}^{\infty} \frac{d\xi e^{-\xi^2\mu}}{\xi^2 + \beta^2} \sin z\xi = 0$ since it is an odd function.

and $\displaystyle\int_{-\infty}^{\infty} \frac{d\xi \ e^{-\mu\xi^2}}{\xi^2 + \beta^2} \cos(z\xi) = 2 \int_{0}^{\infty} \frac{d\xi e^{-\mu\xi^2}}{(\xi^2 + \beta^2)} \cos(z\xi)$

by virtue of its "evenness."

Thus

$$2 \int_{0}^{\infty} \frac{d\xi \ e^{-\mu\xi^2}}{(\xi^2 + \beta^2)} \cos(z\xi) = 2 \left\{ \frac{1}{2} \int_{0}^{\infty} d y \ g(y) \ f(|x-y|) + \right.$$

$$\left. \frac{1}{2} \int_{0}^{\infty} d y \ g(y) \ f(x+y) \right\}$$

where, using the result given on pg. 9, <u>Tables of Integral Transforms</u>, (Erdelyi, Magnus, Oberhettinger, Tricomi) we have

$$g(y) = \sqrt{\frac{\pi}{2}} \int_{0}^{\infty} d\xi \ \frac{\cos(\xi y)}{\xi^2 + \beta^2} = \sqrt{\frac{\pi}{2}} \ \frac{1}{\beta} \ e^{-\beta y}.$$

This can be evaluated explicitly.

Also, we have

$$f(y) = \sqrt{\frac{\pi}{2}} \int_{0}^{\infty} d\xi \ e^{-\mu\xi^2} \cos(z\xi) = \frac{1}{\sqrt{2\mu}} \ \exp\left[-\left(\frac{z}{2\sqrt{\mu}}\right)^2\right]$$

Thus

$$g(y) = \sqrt{\frac{\pi}{2}} \frac{1}{\beta} \; e^{-\beta y}$$

and

$$f(z \pm y) = \frac{1}{\sqrt{2\mu}} \; e^{-\left[\frac{z \pm y}{2\sqrt{\mu}}\right]^2}.$$

We let

$$I_1 = \frac{1}{2} \frac{1}{\beta} \sqrt{\frac{\pi}{2}} \frac{1}{\sqrt{2\mu}} \int_0^\infty d y \; e^{-\beta y - \left[\frac{z-y}{2\sqrt{\mu}}\right]^2}$$

and

$$I_2 = \frac{1}{2} \frac{1}{\beta} \sqrt{\frac{\pi}{2}} \frac{1}{\sqrt{2\mu}} \int_0^\infty d y \; e^{-\beta y - \left[\frac{z+y}{2\sqrt{\mu}}\right]^2}$$

so that

$$\int_0^\infty d\xi \; \frac{e^{-\mu \xi^2} \cos z\xi}{\xi^2 + \beta^2} = I_1 + I_2.$$

Then let

$$I_3 = \int_0^\infty d y \; e^{-\beta y - \left(\frac{z-y}{2\sqrt{\mu}}\right)^2}$$

$$I_4 = \int_0^\infty d y \; e^{-\beta y - \left(\frac{z+y}{2\sqrt{\mu}}\right)^2}.$$

In addition, we note that

$$\beta y + \left[\frac{z+y}{2\sqrt{\mu}}\right]^2 = \left(\frac{y}{2\sqrt{\mu}} + \beta\sqrt{\mu} + \frac{z}{2\sqrt{\mu}}\right)^2 + \left(\frac{z}{2\sqrt{\mu}}\right)^2 - \left(\beta\sqrt{\mu} + \frac{z}{2\sqrt{\mu}}\right)^2$$

$$\beta y + \left[\frac{z-y}{2\sqrt{\mu}}\right]^2 = \left(\frac{y}{2\sqrt{\mu}} + \beta\sqrt{\mu} - \frac{z}{2\sqrt{\mu}}\right)^2 + \left(\frac{z}{2\sqrt{\mu}}\right)^2 - \left(\beta\sqrt{\mu} - \frac{z}{2\sqrt{\mu}}\right)^2.$$

Accordingly

$$I_3 = e^{-\left(\frac{z}{2\sqrt{\mu}}\right) + \left(\beta\sqrt{\mu} + \frac{z}{2\sqrt{\mu}}\right)^2} \int_0^\infty d y \; e^{-\left(\frac{y}{2\sqrt{\mu}} + \beta\sqrt{\mu} \frac{z}{2\sqrt{\mu}}\right)^2},$$

while

$$I_4 = e^{\left(\frac{z}{2\sqrt{\mu}}\right)^2 + \left(\beta\sqrt{\mu} + \frac{z}{2\sqrt{\mu}}\right)^2} \int_0^\infty dy \; e^{-\left(\frac{y}{2\sqrt{\mu}} + \beta\sqrt{\mu} - \frac{z}{2\sqrt{\mu}}\right)^2}.$$

We let

$$I_5 = \int_0^\infty dy \; e^{-\left(\frac{y}{2\sqrt{\mu}} + \beta\sqrt{\mu} + \frac{z}{2\sqrt{\mu}}\right)^2}$$

$$I_6 = \int_0^\infty dy \; e^{-\left(\frac{y}{2\sqrt{\mu}} + \beta\sqrt{\mu} - \frac{z}{2\sqrt{\mu}}\right)^2}.$$

Next we make the substitutions:

$$\eta = \frac{y}{2\sqrt{\mu}} + \beta\sqrt{\mu} + \frac{z}{2\sqrt{\mu}}$$

$$d\eta = \frac{dy}{2\sqrt{\mu}}$$

and we have

$$I_5 = 2\sqrt{\mu} \int_{\beta\sqrt{\mu} + \frac{z}{2\sqrt{\mu}}}^\infty d\eta \; e^{-\eta^2} = 2\sqrt{\mu} \left\{ \frac{\sqrt{\pi}}{-z} \left[\left(1 - \text{erf}\left(\beta\sqrt{\mu} + \frac{z}{2\sqrt{\mu}}\right)\right]\right\}$$

$$I_5 = \sqrt{\pi\mu} \left[1 - \text{erf}\left(\beta\sqrt{\mu} + \frac{z}{2\sqrt{\mu}}\right) \right]$$

while

$$I_6 = \sqrt{\pi\mu} \left[1 - \text{erf}\left(\beta\sqrt{\mu} - \frac{z}{2\sqrt{\mu}}\right) \right]$$

$$I_3 = \sqrt{\pi\mu} \exp\left\{ -\left(\frac{z}{2\sqrt{\mu}}\right)^2 + \left(\beta\sqrt{\mu} + \frac{z}{2\sqrt{\mu}}\right)^2 \right\} \left\{ 1 - \text{erf}\left(\beta\sqrt{\mu} + \frac{z}{2\sqrt{\mu}}\right) \right\}$$

$$I_3 = \sqrt{\pi\mu} \exp\left\{ -\left(\frac{z}{2\sqrt{\mu}}\right)^2 + \left(\beta\sqrt{\mu} - \frac{z}{2\sqrt{\mu}}\right)^2 \right\} \left\{ 1 - \text{erf}\left(\beta\sqrt{\mu} - \frac{z}{2\sqrt{\mu}}\right) \right\}$$

or

$$I = I_1 + I_2 = \frac{\pi}{4\beta} \; e^{-\left(\frac{z}{2\sqrt{\mu}}\right)^2} \left\{ e^{\left(\beta\sqrt{\mu} + \frac{z}{2\sqrt{\mu}}\right)^2} \left[1 - \text{erf}\left(\beta\sqrt{\mu} + \frac{z}{2\sqrt{\mu}}\right) \right] \right.$$

$$\left. + e^{\left(\beta\sqrt{\mu} - \frac{z}{2\sqrt{\mu}}\right)^2} \left[1 - \text{erf}\left(\beta\sqrt{\mu} - \frac{z}{2\sqrt{\mu}}\right) \right] \right\}$$

if $\left(\frac{z}{2\sqrt{\mu}}\right) \ll 1$ and $\beta\sqrt{\mu} > \frac{z}{2\sqrt{\mu}}$, then

$$F(z) = \frac{\pi}{4\beta} \; e^{-\left(\frac{z}{2\sqrt{\mu}}\right)^2} \; 2 \, e^{(\beta\sqrt{\mu})^2} \left\{ 1 - \text{erf} \, (\beta\sqrt{\mu}) \right\}$$

and we have

$$F(z) = \frac{\pi}{2\beta} \left[1 - \text{erf} \, (\beta\sqrt{\mu}) \right] \; e^{-\left(\frac{z}{2\sqrt{\mu}}\right)^2} \sim e^{-\left(\frac{z}{2\sqrt{\mu}}\right)^2}. \tag{58}$$

Then, if $\frac{z}{2\sqrt{\mu}} > 1$, we have

$$F(z) \rightarrow 2 \int_0^\infty d\xi \; \frac{\cos z \, \xi}{\xi^2 + \beta^2} = \frac{2}{\beta} \; e^{-\beta z} \sim e^{-\beta z}, \tag{59}$$

It has been derived in equation (58) that, for small values of z, the flux will fall off as $e^{-k_1 z^2}$. For larger values of z, equation (59) demonstrates a flux dependency of $e^{-k_2 z}$.